NATIONAL AERONAUTICS AND SPACE ADMINISTRATION

Technical Report 32-1112

The Formation and Properties of Liquid Sheets Suitable for use in Rocket Engine Injectors

Robert W. Riebling

Approved by:

D. Dipprey, Manager
Liquid Propulsion Section

JET PROPULSION LABORATORY

CALIFORNIA INSTITUTE OF TECHNOLOGY

PASADENA, CALIFORNIA

June 15, 1967

TECHNICAL REPORT 32-1112

Acknowledgment

The author wishes to acknowledge with sincere thanks the contributions of the following persons to this research:

Dr. Duane F. Dipprey for his many thoughtful suggestions concerning dimensional analysis and the development of generalized correlations; Mr. Bruce H. Johnson for conceiving the impinging-sheet concept, and Messrs. David D. Evans and Walter B. Powell for conducting the initial development effort on the impinging-sheet and cup-and-plug injector elements, respectively; it was the promise shown by these devices that led to the present attempt to better understand sheet formation and behavior.

The author is also indebted to Messrs. Gary M. Mendles, Walter Buckholtz, and Elmer A. Smith, Liquid Propulsion Section technicians, for carrying out the experimental portions of this program.

Contents

Contents (contd)

Tables

Figures

Contents (contd)

Abstract

When a jet of liquid from a circular orifice is directed tangentially against a concave cylindrical surface, it spreads to form a thin, flat sheet of liquid. Such sheets can be used in several different kinds of liquid propellant rocket engine injectors.

An applied research program was conducted to determine the properties of sheets formed in this manner, as well as the conditions necessary to the formation of suitable sheets. Sheet dimensions and spatial orientation, and the distributions of mass and velocity across the flowing sheets were measured, using three inert propellant simulants. All of these sheet parameters were correlated in terms of the geometry of the sheet formation devices. Injection velocity, propellant physical properties, and the absolute sizes of these devices were found to exert only second-order effects. Distributions of thickness and momentum flux were also obtained and correlated. All sheet properties were found to be scalable because of geometric and dynamic similarity, and can now be predicted and controlled with a high degree of confidence.

The Formation and Properties of Liquid Sheets
Suitable for use in Rocket Engine Injectors

I. Introduction

Although impinging-jet elements (both like and unlike) have been used successfully for many years in liquid bipropellant rocket engine injectors, they exhibit a number of disadvantages that can impair their effectiveness in certain applications. For example, the performance of an individual element is sensitive to the accuracy of alignment of the impinging jets, while the uniformity of combustion in a multielement injector depends on the reproducibility of that alignment from one element to the next. Thus, manufacturing tolerances are important considerations and may become critical limitations. In addition, it is frequently necessary to make impinging-jet elements quite small in order to achieve satisfactory combustion efficiency. This is true for several reasons. First, the mean droplet size in a spray from a pair of impinging jets was shown by Ingebo at NACA to decrease as the three-halves power of the jet diameter, at constant mass flow rate (Ref. 1). Hence, the degree of atomization upon which efficient combustion depends should improve as the orifice diameter is decreased. This has been verified experimentally by many different investigators.

More important, however, is the fact that for extremely reactive storable propellants, such as nitrogen tetroxide

(N_2O_4) and hydrazine (N_2H_4), rapid chemical reaction may occur at the liquid interface between unlike-impinging jets. The resultant gases can disrupt the streams before effective liquid-phase mixing has occurred, considerably lowering the combustion efficiency attainable. The work of Johnson and Stanford at JPL (Refs. 2 and 3) shows that the magnitude of this effect increases sharply with the diameters of the unlike impinging jets. Thus, impinging-jet injectors must often employ a multiplicity of very small diameter elements to achieve high performance, thereby increasing their complexity.

In the light of these inherent disadvantages, considerable effort at this Laboratory has been devoted to the development of simple injector elements (which do not employ impinging jets) for use with hypergolic storable propellants. One such class of injector incorporates thin, flat sheets of propellant. The use of sheets in liquid rocket engine injection devices is, of course, not new. Sheets have been formed in the past by forcing the propellants through narrow slots, but this technique has generally been limited by the sensitivity of the sheet properties to the geometry, manufacturing tolerances, and surface finish of the slots. Narrow slots or annuli are also prone

to clogging by accumulated particulate matter. The desirability of forming a sheet on some device *external* to a more conventional and better-controlled (round) orifice is readily apparent.

One such sheet-formation method is the tangential impingement of round jets on a curved surface, as shown in Fig. 1. This technique has been used for some time in commercially-available[1] spray nozzles, and so is not novel in itself. But because of the unique properties of the sheets formed by this method, its application to rocket engine injectors is an innovation which promises unprecedented control of the combustion process. The device shown schematically in Fig. 1 should not be confused with members of the various genera of so-called "splash plate" injectors, which characteristically impinge fuel and oxidizer, either singly or in combination, in a non-tangential manner against some solid surface, where considerable splashing or splattering is intended to take place.

In the configuration of Fig. 1, the jet issuing from the orifice turns smoothly onto the deflector surface with a

[1]Spraying Systems Co., 3201 Randolph Street, Bellwood, Illinois. Bete Fog Nozzle, Inc., 309 Wells Street, Greenfield, Massachusetts, among others.
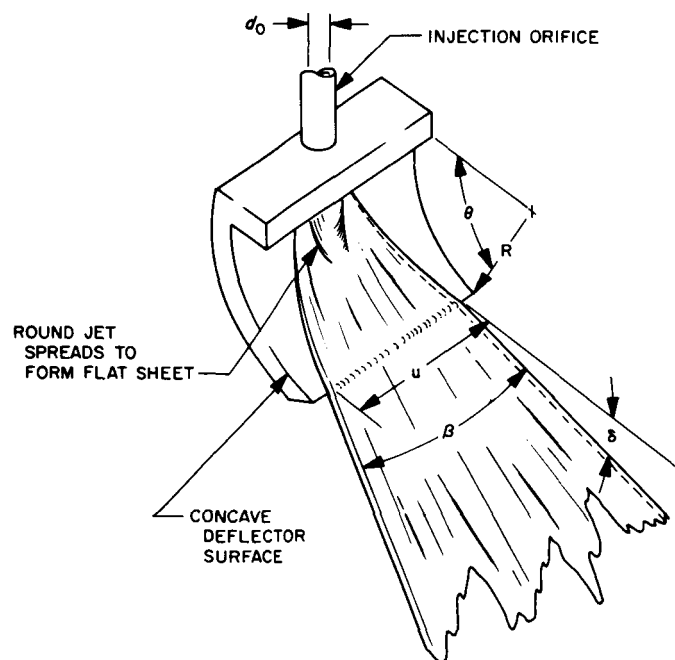
Fig. 1. Schematic representation of sheet formation on a deflector

gradual transition to a thin liquid sheet of width w. No splashing occurs. Upon leaving the deflectors, the free sheets spread through an angle β before finally breaking up into droplets. In general, the sheets do not exit tangentially. Rather, the axes of the sheets are deflected through a negative angle δ away from the deflector surface tangents, as shown in Fig. 1. This angle δ will be termed the *deflection* angle in this report. It should not be confused with the *deflector* angle θ, which has been machined into the deflector. The net angular change in direction of the stream away from its original axis is therefore the *deflector* angle θ less the *deflection* angle δ. The curved surfaces may be simple concave cylinders, composites of cylindrical and plane surfaces, or more complex shapes. Normally, only the first two classes of surface would be chosen to facilitate manufacture.

The deflection of liquid streams in the manner described can be used to form sheets in rocket engine injector elements. A typical injector would have a number of these elements oriented so as to control the interactions between adjacent sheets, yield the desired mass and mixture ratio distributions across the injector face, and provide a uniform circumferential combustion chamber heat flux pattern.

One important application is the impinging-sheet unlike doublet injector element (Ref. 4), in which the resultant sheets are planar (Fig. 2). One advantage of this design is its relative insensitivity to misimpingement due to manufacturing tolerances.

Thin sheets are also exploited in the so-called "cup-and-plug" injector, shown in Fig. 3 and described in Ref. 5, a device successfully fired with both ClF_3/N_2H_4 and LO_2/LH_2. It is a variation of the conventional showerhead concept, retaining all its advantages. However, the use of thin sheets of propellant can provide the same surface area for propellant vaporization as in a showerhead injector of comparable thrust level, but with considerably fewer orifices. Also, the holes may be grouped into small circular elements which can be fabricated independently and then incorporated into a larger injector assembly. This injector produces sheets with a slight degree of circumferential curvature. Both kinds of element also provide a degree of film cooling to the injector face.

The key spray parameters which influence combustion efficiency in any injector are propellant mixing, atomization and vaporization. Different physical processes may govern the magnitude and relative uniformity of these

Fig. 2. Typical impinging-sheet injector element

Fig. 3. Schematic representation of a cup-and-plug injector

geometry, propellant physical properties, and injection velocity. The influence of such secondary factors as deflector surface conditions, orifice length-to-diameter ratio, and deflector size (scaling effects) also must be known. All these are variables more readily controlled by the designer than "mixing" and "atomization." In addition, it was necessary to define those conditions under which stable sheets, with properties making them suitable for use in injector applications, are formed.
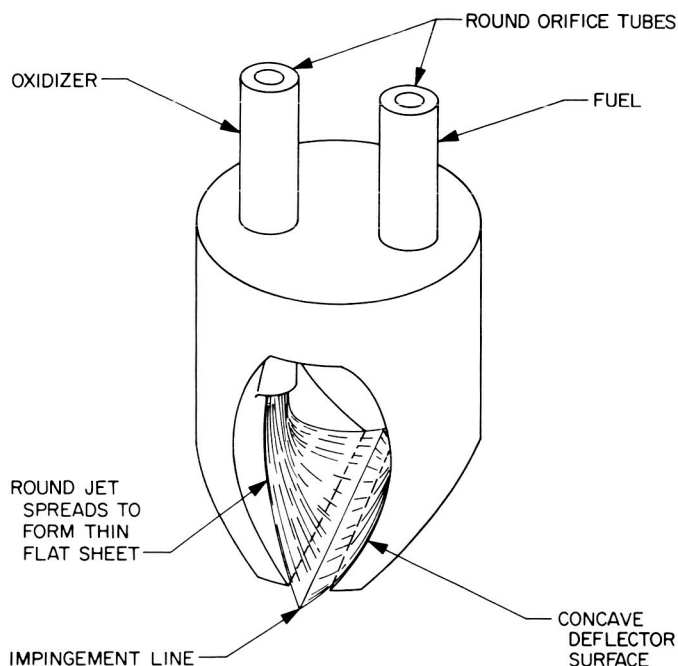
This report presents the results of an applied research program to determine these effects. All work was carried out with single deflector/orifice combinations, rather than with specific injector elements, and non-reactive propellant simulants were used to facilitate direct measurement of sheet properties. The results, which permit the prediction and control of the key sheet properties, are directly applicable to the design of any injector based on the principle of tangential impingement of round jets on concave, cylindrical deflectors.

II. Apparatus and Procedures

A. Experimental Sheet-Formation Apparatus

A typical sheet-formation device is shown schematically in Fig. 1. Concave cylindrical deflector surfaces of radius R and included angle θ were machined into aluminum blocks and polished to a surface finish of about 25 micro-in. (rms). Circular-cross-section injection orifices of inside diameter d_0 were positioned such that the liquid propellant simulants were introduced tangentially to the deflector surfaces.

Two different sizes of apparatus were used. The majority of experiments was conducted with devices the size of typical injector elements: radii ranging between 0.1 and 0.7 in., orifice diameters of 0.018 to 0.040 in., and deflector angles of 15 to 45 deg. Much larger sheet-formation devices were also used in a limited number of experiments to determine if the results obtained with the smaller apparatus were scalable. The latter had 6.5-in. radii, deflector angles of 15, 30, and 45 deg, and orifice diameters of 0.405 in. These larger diameters extended the range of Reynolds and Weber numbers of the orifice flow by nearly a full order of magnitude.

Inert propellant simulants were introduced to the deflectors through the injection orifices. Reynolds numbers ranging from about 1×10^4 to 3×10^5, and Weber numbers of about 10 to 1000 were obtained by systematically varying the injection velocity (50 to 137 ft/sec), the fluid

factors in the cup-and-plug and unlike impinging-sheet injectors. However, in both cases these properties of the resulting sprays should be related to the dimensions and spatial orientation of the free-flowing sheets from which they are formed, and to the distributions of mass flux, fluid velocity, fluid momentum and thickness within each individual sheet. Thus, intelligent design of any kind of sheet injector is predicated upon (although not necessarily limited to) a knowledge of the manner in which the sheet dimensions, and the velocity, mass, and momentum profiles, vary with such primary parameters as deflector

physical properties (by changing fluids), and the orifice diameters. A wide range of physical properties was realized through the use of water, trichlorethylene, and n-hexane as the test fluids; their properties are summarized in Table 1.

Table 1. Physical properties of propellant simulants

Liquid	Density, lbm/ft³	Viscosity, lbm/ft-sec × 10⁴	Surface tension, lbf/ft × 10³
Water	62.4	6.7	5.0
Trichlorethylene	90.5	3.7	2.0
n-Hexane[a]	43.3	2.4	1.5

[a]Commercial grade. Data are Laboratory measurements.

It is generally recognized that fully-developed turbulent flow is necessary to assure complete hydraulic reproducibility (as characterized by stability, similarity and symmetry) in jets issuing from round orifices (Ref. 6). It was therefore expected that the degree of developed orifice turbulence would likewise influence the flow characteristics of any sheets formed from such round jets.

There are two basic requirements that must be met in order to assure fully developed turbulent flow. The first of these, of course, is that the Reynolds number, Re, must exceed about 2100. The second is sufficient orifice tube length, which is required if fully turbulent velocity profiles are to develop. The first condition was met by using the Reynolds number range mentioned above. In order to assess the effect of orifice length, two different sets of orifices were employed in the experiments made to measure sheet dimensions and orientation. The majority of tests were conducted with "short" orifices (drilled holes) with length-to-diameter ratios ranging between 6 and 12. These were typical of current state-of-the-art drilled-hole orifices, in which fully-developed turbulent flow is not usually attained. For comparison purposes, a number of the experiments were repeated with "long" orifices — straight lengths of stainless steel tubing with length-to-diameter ratios of 110 — to assure fully-developed turbulent orifice flow with its characteristic hydraulic reproducibility.

All of the "large" flow devices (6.5-in. radii) had orifice length-to-diameter ratios of 100, as did all of the "small" devices used in the measurement of sheet mass and velocity distribution.

B. Measurement of Sheet Dimensions and Spatial Orientation

The sheet width w and spreading angle β were measured from high-speed still photographs of the flowing sheets, made with synchronized-pulse lighting. The lens axis was orthogonal (± 5 deg) to the sheet axis in each case.

The sheet deflection angle δ was measured *in situ* to within about ± 1 deg, as follows. Upon rotation of the entire apparatus, the axis of the flowing sheet (defined as the angle bisector of the sheet as seen edge-on, Fig. 4) was aligned with the vertical by optical techniques. The angle α (Fig. 4) between the bottom surface of the block and the horizontal was then measured, and the deflection angle was found from the relation,

$$\delta = \theta - \alpha \tag{1}$$
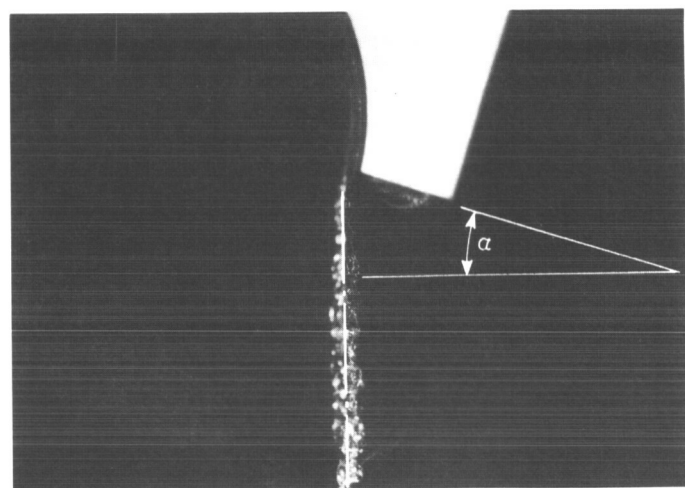
Fig. 4. Typical side view of flowing sheet, showing method of determining the deflection angle

C. Measurement of Sheet Mass and Velocity Distributions

The mass flux per unit width of sheet, $d\dot{w}/dx$, was measured by traversing the width of the sheets with a small, flattened-end tube which collected liquid over a known time interval at each station. This device is shown schematically in Fig. 5. The probe was positioned as close to the edge of the deflector as possible (0.15 in.) without disturbing the sheet formation process. Most of the sheets studied were formed on the small deflectors (0.1- to 0.7-in. radii and 0.018- to 0.040-in. orifice diameter), although a
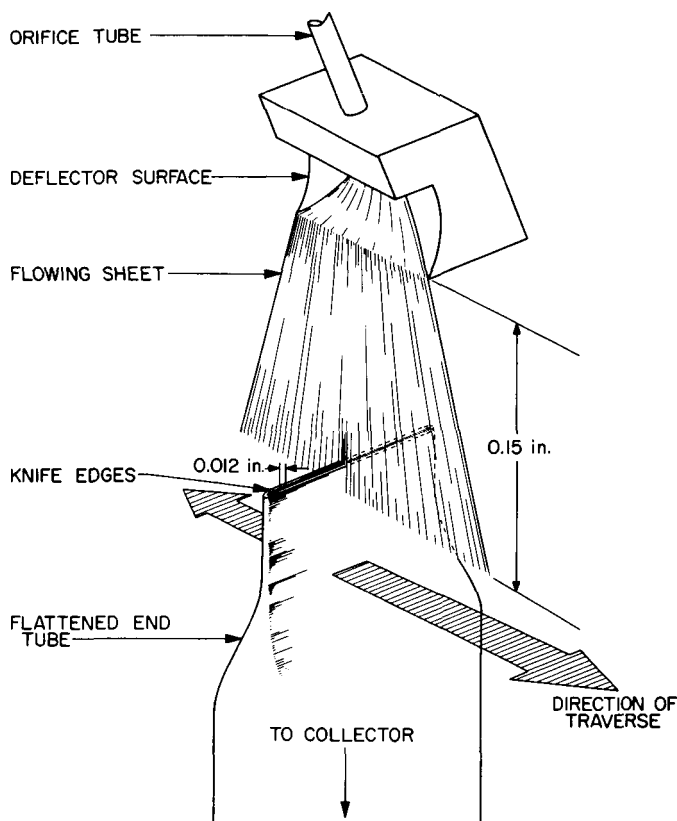
Fig. 5. Schematic representation of mass flow rate distribution apparatus
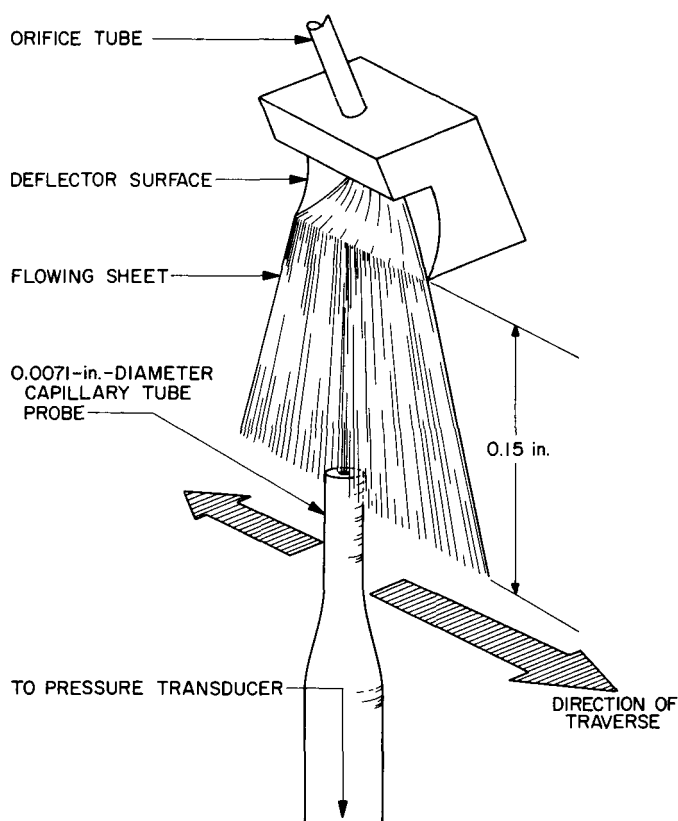
Fig. 6. Schematic representation of apparatus for measuring velocity distribution

few experiments were made on the large deflectors (6.5-in. radii and 0.405-in. orifice diameters) to check the scalability of the results. The test fluids were water and trichlorethylene, flowing at injection velocities ranging between 57 and 142 ft/sec. Corresponding Reynolds numbers ranged between 1.1×10^4 and 3.1×10^5, while Weber numbers varied from 60 to about 360. All orifices used had length-to-diameter ratios of 100, and the deflector angles ranged between 15 and 45 deg.

Dynamic pressure was measured across sheets formed from the same wide variety of deflector/orifice combinations, flowing water and trichlorethylene over Reynolds and Weber number ranges similar to those used in the mass-distribution measurements. A 0.0071-in.-diameter capillary tube probe (Fig. 6) connected to a pressure transducer measured dynamic pressure across the width of each sheet at a distance of 0.15 in. from the edge of the deflector. At each station along the sheet, the probe was also moved in a direction normal to the sheet width to assure that the maximum pressure (velocity head) at

that station was measured. The exit velocity at each position across the sheet was then calculated from

$$V_e = 12 \left[\frac{2g_c \, P_d}{\rho} \right]^{1/2} \tag{2}$$

The distributions of fluid momentum and sheet thickness were not measured directly. Rather, they were calculated from the mass and velocity distribution data by methods to be described in Section III.D.

D. Observation of Sheet Stability

To determine qualitatively the effect of fluid turbulence on the stability of the flowing sheets, high-speed (~7000 frame/sec) motion pictures were made of sheet formation on a number of different deflectors

$$0.33 \lesssim \frac{h}{d_0} \lesssim 4.02$$

Where h, the deflector "overhang," is equal to $R(1-\cos\theta)$ and is the transverse distance to which the deflector protrudes into the otherwise unperturbed jet. Stroboscopic-synchronized illumination was used. Water and hexane were flowed through various diameter ($0.018 \leqq d_0 \leqq 0.040$ in.) orifices at 100 ft/sec. Two different orifice length-to-diameter ratios were again employed. In one test series, drilled holes with length-to-diameter ratios between 6 and 12 were used; in the other, the liquids were introduced to the deflectors via tubing with straight-run length-to-diameter ratios of 100. In the setup of the flow apparatus, care was taken to eliminate feed system interactions which might have introduced extraneous instabilities.

III. Experimental Results

A. Visual Properties of Sheets

Detailed examination of the more than 200 sheet photographs taken during the course of this investigation permitted the classification of sheets into three distinct flow categories, based on their appearance alone. Figure 7 shows the visual properties of typical sheets in each category, produced by the tangential introduction of water at 65 ft/sec onto deflectors of different h/d_0. Similar results were obtained with water at other velocities; the deflector/orifice geometry seems to determine the visual characteristics of the sheets.

In the first category, arbitrarily designated "A" (Fig. 7a), the sheet has a ragged or feathered appearance. Its physical boundaries are ill-defined, and in many respects it resembles an imperfectly formed round jet more than it does a flat sheet. The "sheets" generally looked this way when the deflectors were very short compared to the orifice diameters; that is, when $0 < h/d_0 < 0.75$ and $0 < L/d_0 < 4$. (The arc-length L is equal to $\theta\pi R/180$ when θ is expressed in degrees.)

With longer deflectors, well-formed sheets of the second, or "B" category (Fig. 7b), are formed. These are characterized by well-defined, relatively straight boundaries, and small positive values of the spreading angle β. This kind of sheet was generally formed when $h/d_0 > 0.75$ and $4 < L/d_0 < 13$.

However, as the deflectors are made still longer relative to the orifice diameters, more and more of the available stream energy is apparently dissipated, presumably as friction, so that inertia forces are reduced to the same order of magnitude as surface tension effects. As shown in Fig. 7(c), in this "C" category, the sheet boundaries, although still well-defined, may be more sharply curved, or, in some cases, pinched in (β may be negative in this case). Most of the thickness of the sheet is seemingly concentrated in very pronounced ribs at the edges, and holes repeatedly form and propagate in the thin, film-like central portion. Sheets generally fell in Category C when they were formed on devices with $h/d_0 \gtrsim 5$.

EDGE OF DEFLECTOR

(a) CATEGORY A –
$h/d_0 = 0.5$

(b) CATEGORY B –
$h/d_0 \,\square\, 3.0$

(c) CATEGORY C –
$h/d_0 \,\square\, 12$
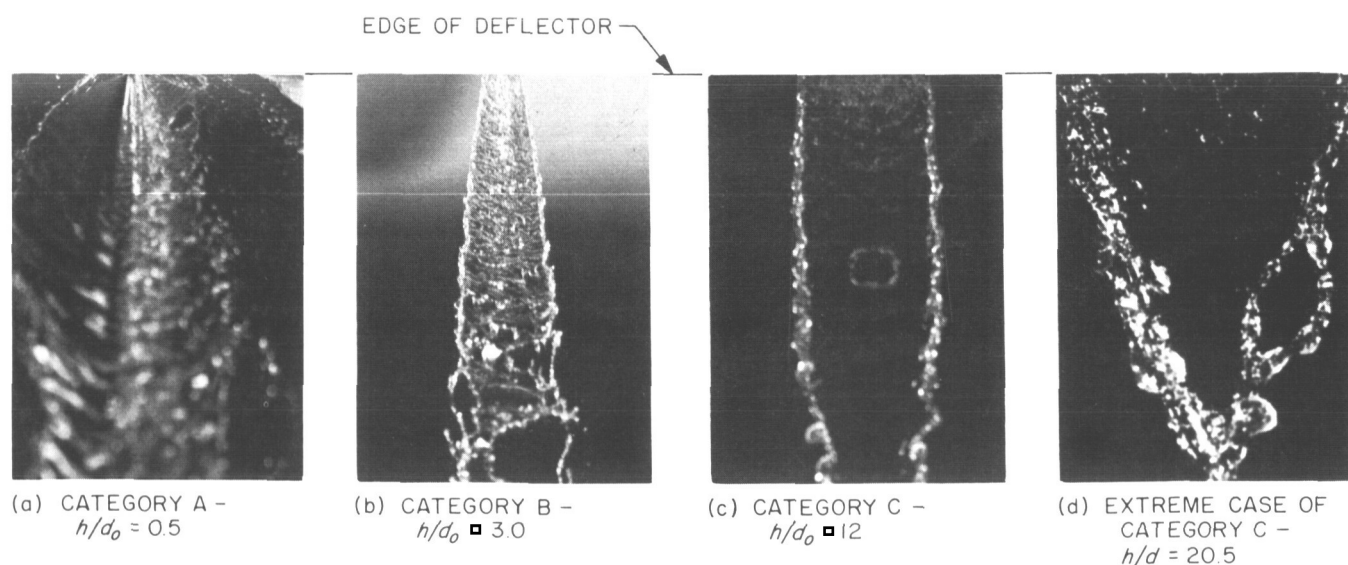
(d) EXTREME CASE OF
CATEGORY C –
$h/d = 20.5$

Fig. 7. Variations in sheet appearance with overhang ratio for water at a constant velocity of 65 ft/sec

An extreme case of Category C is shown in Fig. 7d, where surface tension forces are seen to completely dominate all other forces. The sheets break up into large ligaments immediately upon leaving the deflectors, and large, chunky droplets are produced at the confluence of these ligaments downstream. High negative values of β are typical.

Sheets formed under the same conditions with trichlorethylene and n-hexane appeared almost identical to the water sheets shown in Fig. 7. However, the holes formed when the Category C sheets began to break up were considerably smaller, giving the disintegrating sheets a lacey appearance. In addition, many of the trichlorethylene and n-hexane sheets were seen to shed ligaments from the edges (Fig. 8), an effect not noted with water.
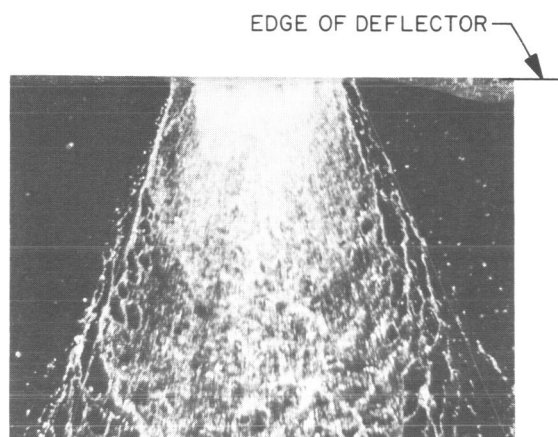
Fig. 8. Ligament shedding by a category B trichlorethylene sheet

With the single exception of these disintegration patterns, no effects of fluid physical properties or injection velocity on the visual characteristics of the sheets could be found. The deflector geometry alone appeared to determine the category into which each sheet could be classified.

The extent of the A and B categories is indicated in Fig. 9, which also presents graphically the relationships between h/d_0, L/d_0, R/d_0, and θ over the range of experimentation. All ill-formed "sheets" with the appearance of Fig. 7(a) fell in the shaded region of Fig. 9, regardless of fluid properties or injection velocity. Similarly, all Category B sheets fell in the open region of Fig. 9. The boundaries of Category C are not shown on Fig. 9, because other evidence, to be introduced subsequently, showed that the differences between the B and C
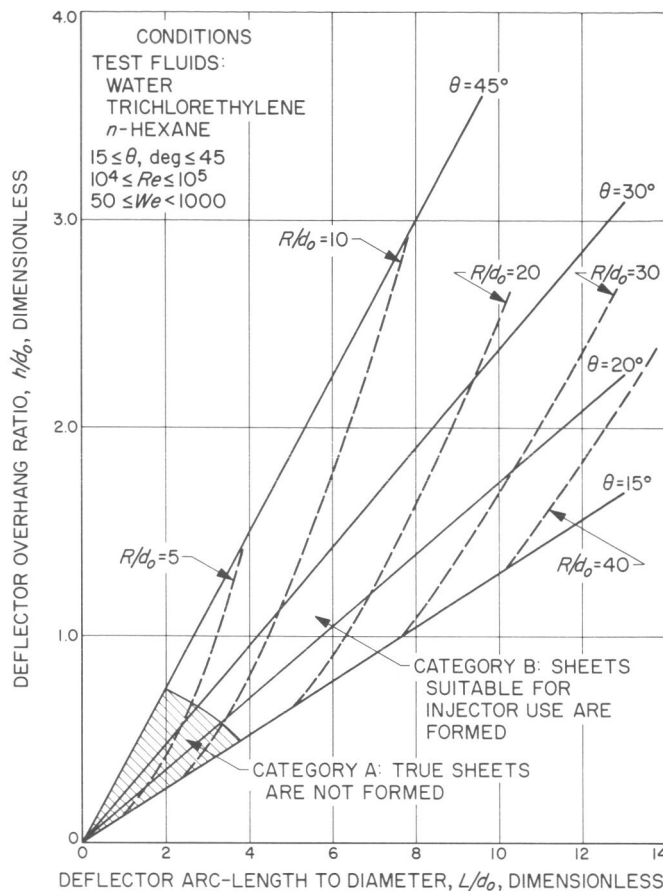
Fig. 9. Effect of deflector geometry on sheet formation

regions were those of degree, rather than of kind. However, the measurement of other flow properties indicated that A and B represented two truly different sheet-flow regimes.

B. Sheet Dimensions and Orientation

Nearly 200 individual experiments were conducted to measure the width w, spreading angle β, and deflection angle δ of flowing sheets, using the liquids, apparatus and procedures previously described.

1. Sheet width. Initially, good correlations were obtained when w/d_0 was plotted vs R/d_0 for a particular fluid at constant injection velocity. An example is presented in Fig. 10 for water flowing at 129 ft/sec. Typically, a family of lines (one line for each value of θ) of slope = ½ resulted at each velocity.

It was subsequently discovered that the effects of the deflector angle θ could be normalized out by plotting
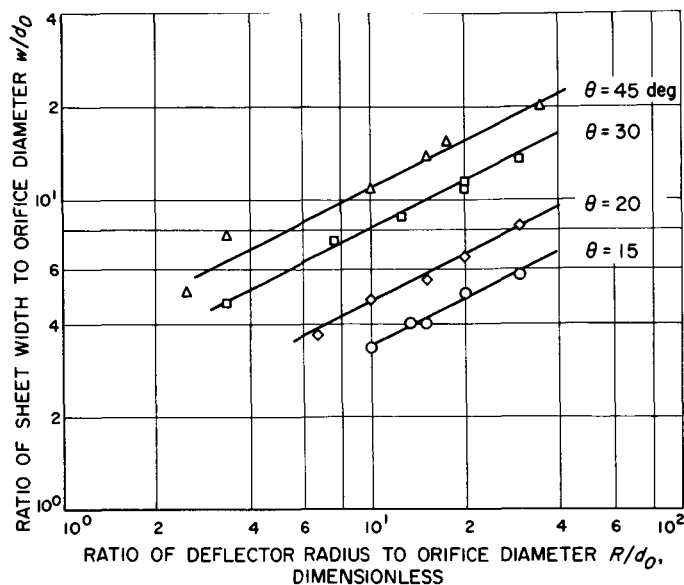
Fig. 10. Variation of dimensionless sheet width parameter with deflector and orifice geometry for water at 129 ft/sec

Fig. 11. Typical variation of ratio of sheet width to orifice diameter with deflector overhang ratio for a single liquid at constant injection velocity

w/d_0 vs h/d_0, instead of R/d_0 (h, the deflector "overhang" is defined as $h = R (1 - \cos \theta)$, and represents the transverse distance the deflector protrudes into the otherwise unperturbed jet). The results of treating the data in this manner are typified by the plot of Fig. 11, which shows how w/d_0 varies with h/d_0 for n-hexane flowing at a constant velocity of 112 ft/sec.

Similar plots were obtained for all three liquids over the entire range of velocities studied. In each case, it was found that

$$\frac{w}{d_0} = A \left(\frac{h}{d_0}\right)^{0.5} \qquad (3)$$

where $5.6 < A < 6.6$. The factor of proportionality A in Eq. (3) appeared to increase slightly with injection velocity for water and trichlorethylene (a threefold increase in $\overline{V}$ caused about a 10% increase in A for both liquids). No change in A with velocity could be found for n-hexane. Further, no simple correlation was found between A and the liquid physical properties (density, viscosity, and surface tension), taken either singly or in combination. The variations of A with velocity and physical properties appeared almost random, and in no case were they very large. This suggested that a single, generalized equation which neglected the apparently second-order velocity and physical properties effects might satisfactorily correlate

the sheet width data for these three liquids (and perhaps for most liquids).

Sheet-width data for all three fluids flowed over the entire velocity range are plotted together in Fig. 12. These data represent the combined results of the nearly 200 individual sheet-width experiments, and include data obtained with both the large "scaled-up" deflectors, and the smaller deflectors with the high (110) orifice length-to-diameter ratios. The equation of the best-fit line of Fig. 12 is

$$\frac{w}{d_0} = 5.8 \left(\frac{h}{d_0}\right)^{0.5} \qquad (4)$$

Although the points of Fig. 12 are spread within a band, the scatter of all these data points taken together is only slightly greater than that in each of the individual plots, such as Fig. 11, from which Fig. 12 was prepared by super-position. Thus the spread shown in Fig. 12 results primarily from a corresponding spread in the raw data, rather than from any appreciable errors introduced as a result of neglecting the effects of injection velocity and/or physical properties of the liquid. However, this spread in the raw data is somewhat greater than was expected, based on the estimated accuracy of the experimental measurements alone. It is attributed to a random variation of the sheet properties with time on those deflectors fed by the short orifice tubes. This effect is discussed in a later section of this report, but its significance lies in the fact that the instantaneous values shown on Fig. 12 can be higher or lower than the time-averaged
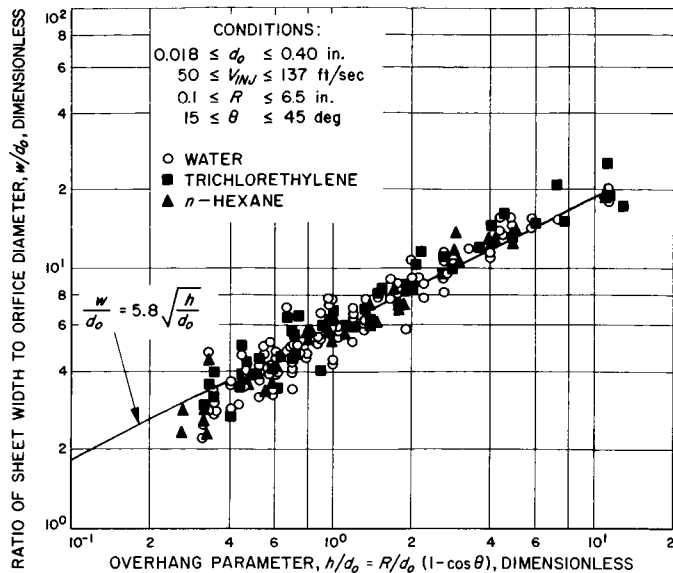
Fig. 12. Ratio of sheet width to orifice diameter as a function of the deflector overhang for three liquids

values, depending on the instant that the photograph from which they were read was taken. Eq. (4), and the straight line on Fig. 12 therefore should correlate the time-averaged values of w/d_0 quite well.

2. Sheet spreading angle. The best method of correlating the sheet spreading angle data for each fluid was found to be a plot of β vs ln (R/d_0) at constant velocity. The results obtained are typified by Fig. 13, which shows all the data for trichlorethylene on the small deflectors with the short orifices. For all three fluids studied, the injector velocity exerted a small but apparently not quite negligible effect on the value of β at constant R/d_0. There were no non-random variations of β with θ or d_0.

The correlation equations found for the three fluids are:

Water:
$$\beta = 104.5 \left[1 + (1.52 \times 10^{-3})\overline{V}\right]$$
$$- 30.7 \ln\left(\frac{R}{d_0}\right) \qquad (5)$$

RATIO OF DEFLECTOR RADIUS TO ORIFICE DIAMETER R/d_0, DIMENSIONLESS
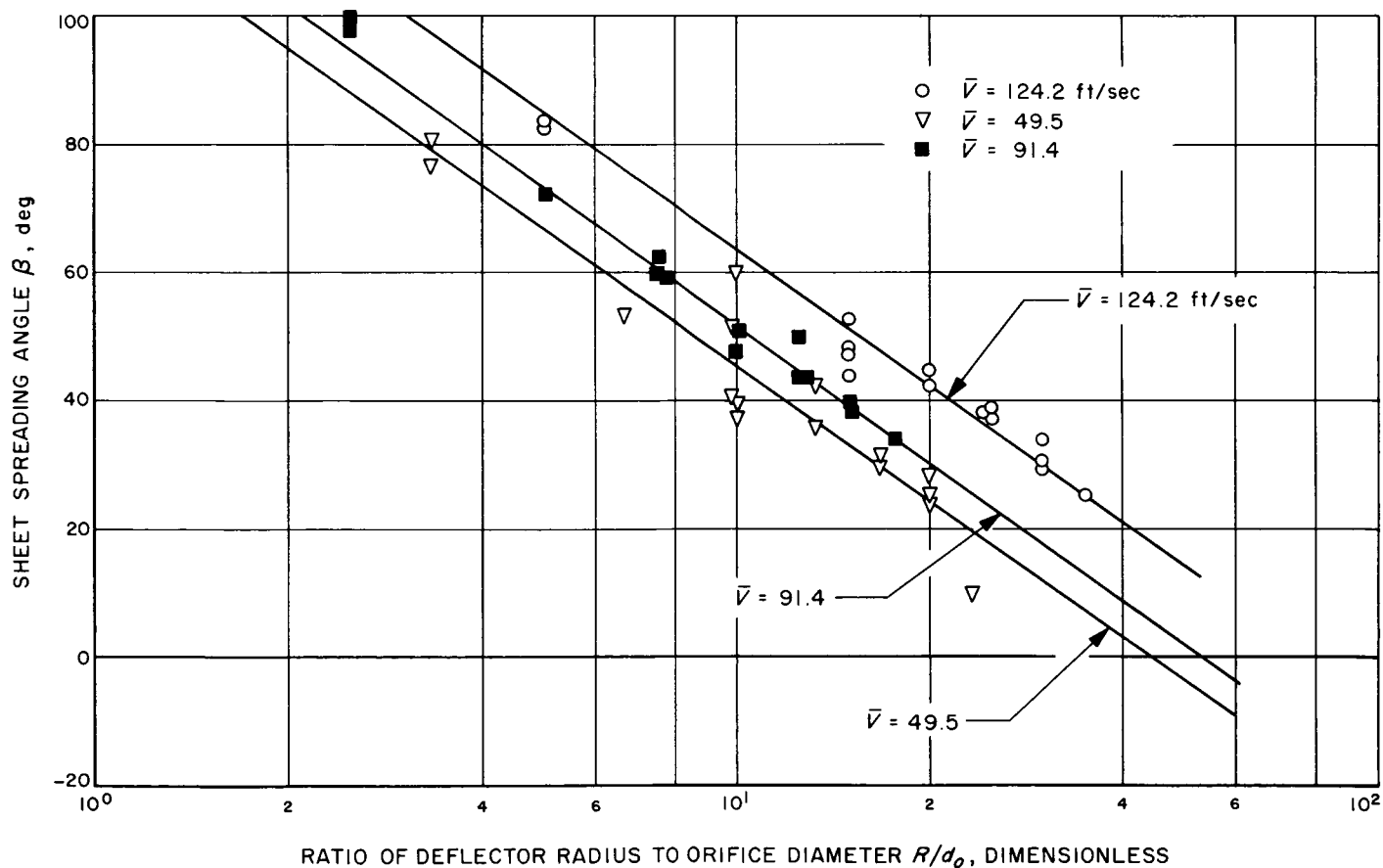
Fig. 13. Effects of deflector geometry and injection velocity on sheet spreading angle for trichlorethylene

Trichlorethylene: $\beta = 108.0\,[1 + (1.52 \times 10^{-3})\overline{V}]$

$$- 30.7\,\ln\left(\frac{R}{d_0}\right) \qquad (6)$$

n-Hexane: $\beta = 110.5\,[1 + (1.52 \times 10^{-3})\overline{V}]$

$$- 30.7\,\ln\left(\frac{R}{d_0}\right) \qquad (7)$$

It is seen that all three equations are of the form

$$\beta = \gamma\,[1 + \epsilon\overline{V}] - k\ln\left(\frac{R}{d_0}\right) \qquad (8)$$

and that all three are identical, except for the value of γ. γ was found to vary with the surface tension of the liquid employed, as shown in Fig. 14.

Equations (5), (6), and (7) correlate the experimental data to within about ± 10 deg, and may be used to pre-
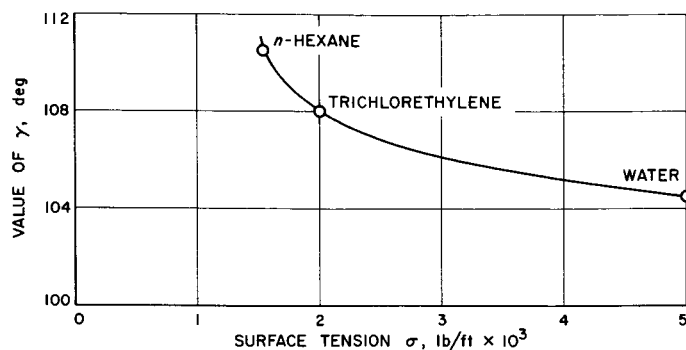
Fig. 14. Effect of liquid surface tension on the value of γ in Eq. (8)

dict the spreading angle for the three inert simulants investigated. For other simulants or propellants, the spreading angle may be estimated from Eq. (8), using $k = 30.7$ deg, $\epsilon = 1.52 \times 10^{-3}$ sec/ft, and γ from Fig. 14. Again, these correlations are for the time-averaged values of the spreading angle.
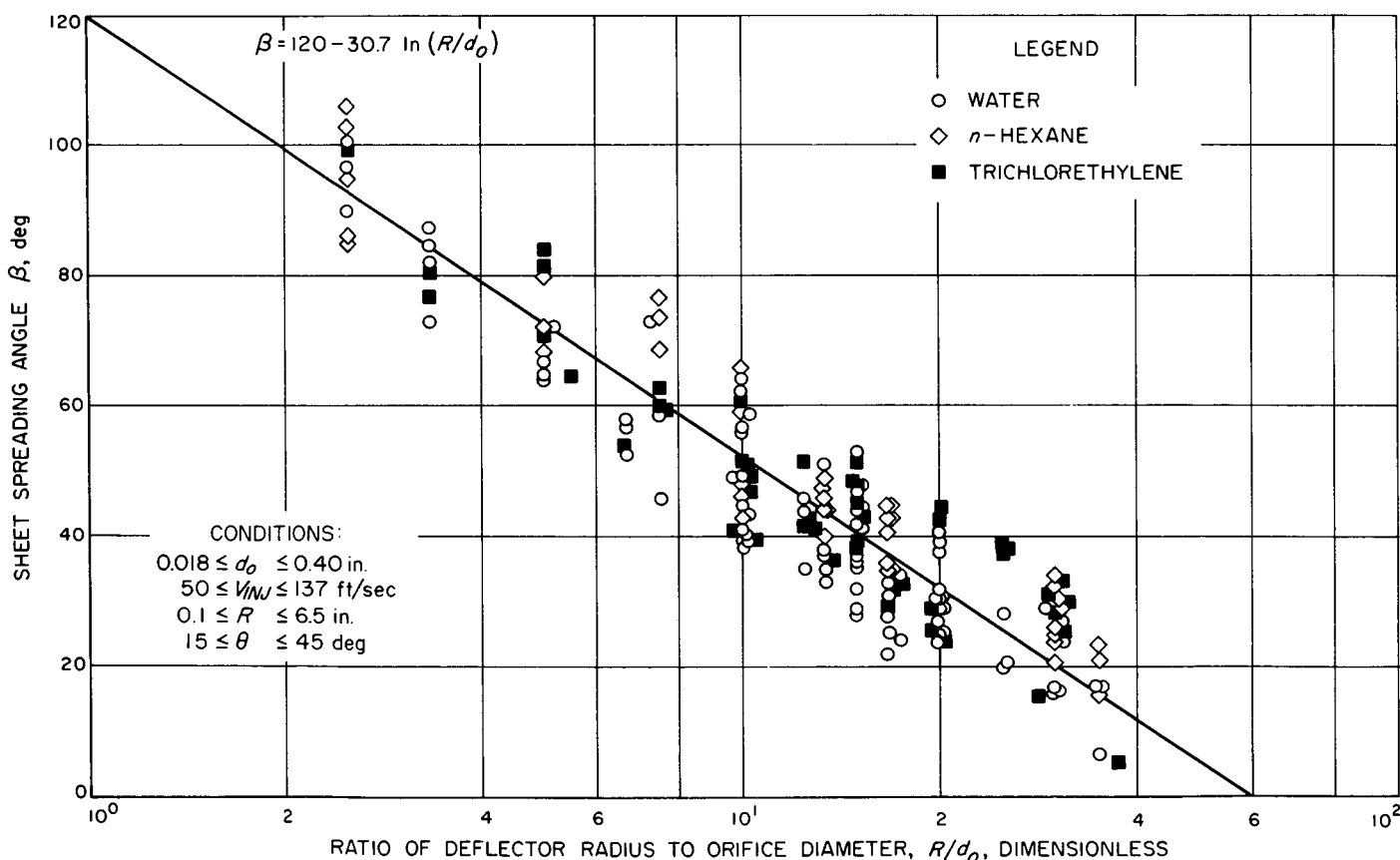
Fig. 15. Effect of deflector geometry on sheet spreading angle for water, trichlorethylene, and n-hexane, $50 \leq \overline{V} \lesssim 137$ ft/sec

As an indication of the relative magnitudes of the geometry and velocity/properties effects in Eq. (8), spreading angle data for all three liquids (the results of the nearly 200 tests) are superimposed without regard to velocity or physical properties in Fig. 15. The graph again includes data obtained with both the large deflectors, and the smaller ones with high orifice length-to-diameter ratios. The major influence is seen to be that of R/d_0 (as already pointed out); the effects of the velocity and property terms are to spread the data into a slightly wider band in this representation. The equation of this generalized curve is

$$\beta = 120 - 30.7 \ln\left(\frac{R}{d_0}\right) \qquad (9)$$

Eq. (9) might be used for rapid estimates or for approximate calculations when exact values of injection velocity and surface tension are not available.

3. Sheet deflection angle. This same technique of considering data for all three liquids simultaneously was applied to the deflection angle with similar results; δ is plotted against h/d_0 in Fig. 16. Attempts were again made to isolate the effects of velocity and physical properties, but no suitable correlation was found, so all data have been included in Fig. 16 without regard to those variables. Since the data scatter is not too great, it can be assumed that velocity and physical properties effects are not very strong.

No simple power-law type correlation was found for δ, owing to its unique variation with h/d_0. δ is very large (on the order of 15 to 25 deg) when h/d_0 is less than about 0.5; it decreases rapidly with increasing h/d_0 until a minimum is reached somewhere between h/d_0 values of about 2 and 6. Further increases in h/d_0 seem to yield only slight increases in δ.

When $h/d_0 = 0$, the circular jet is unperturbed and hence cannot turn ($\delta = 0$). Thus, the curve for very small h/d_0 must be similar to the dashed line shown in Fig. 16, passing through a maximum in the vicinity of $h/d_0 = 0.25$.

Fig. 16. Deflection angle δ versus overhang ratio for three liquids

Fig. 17. Mass flow-rate distributions in free sheets of water at constant injection velocity as functions of deflector angle and overhang ratio

C. Sheet Mass and Velocity Distributions

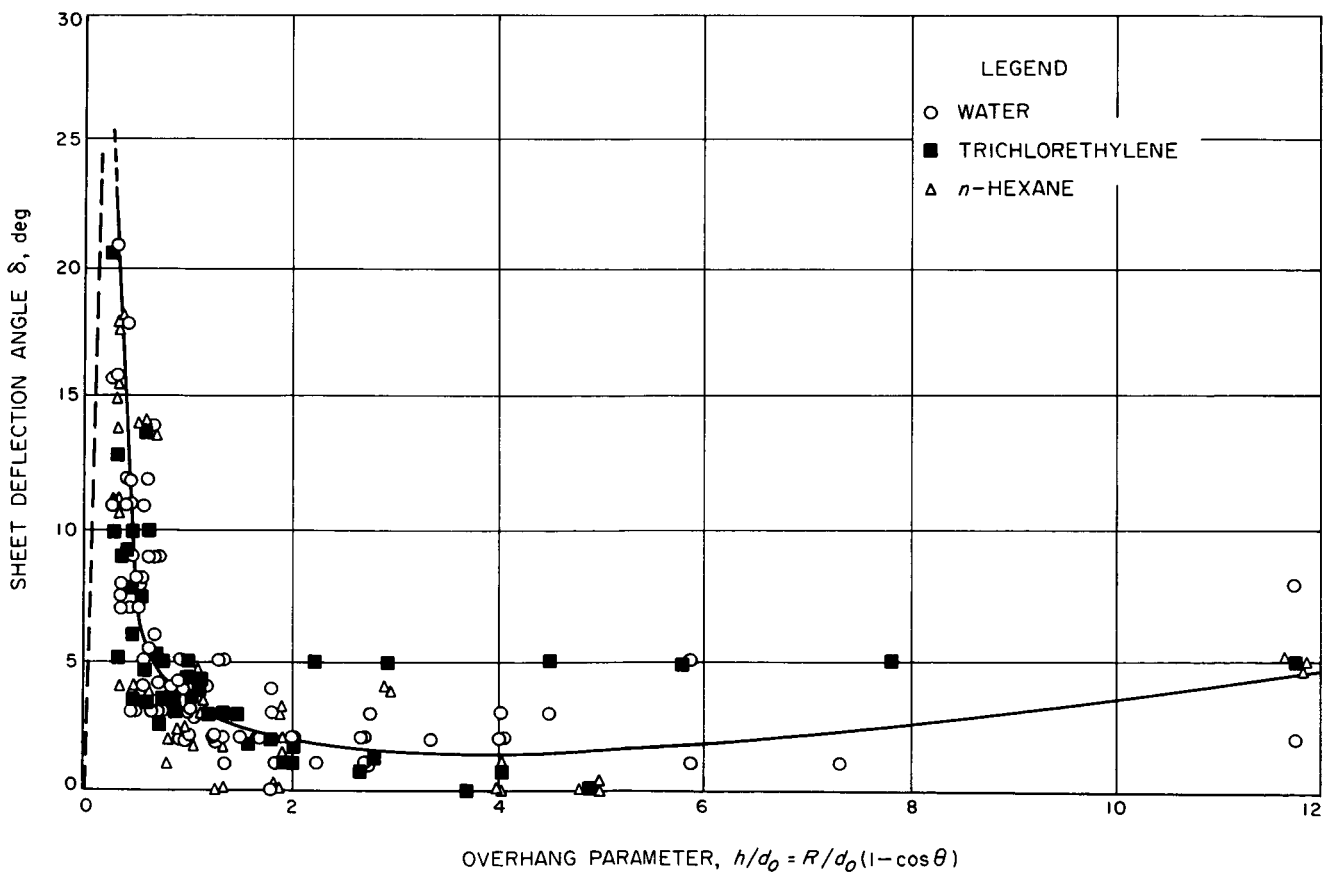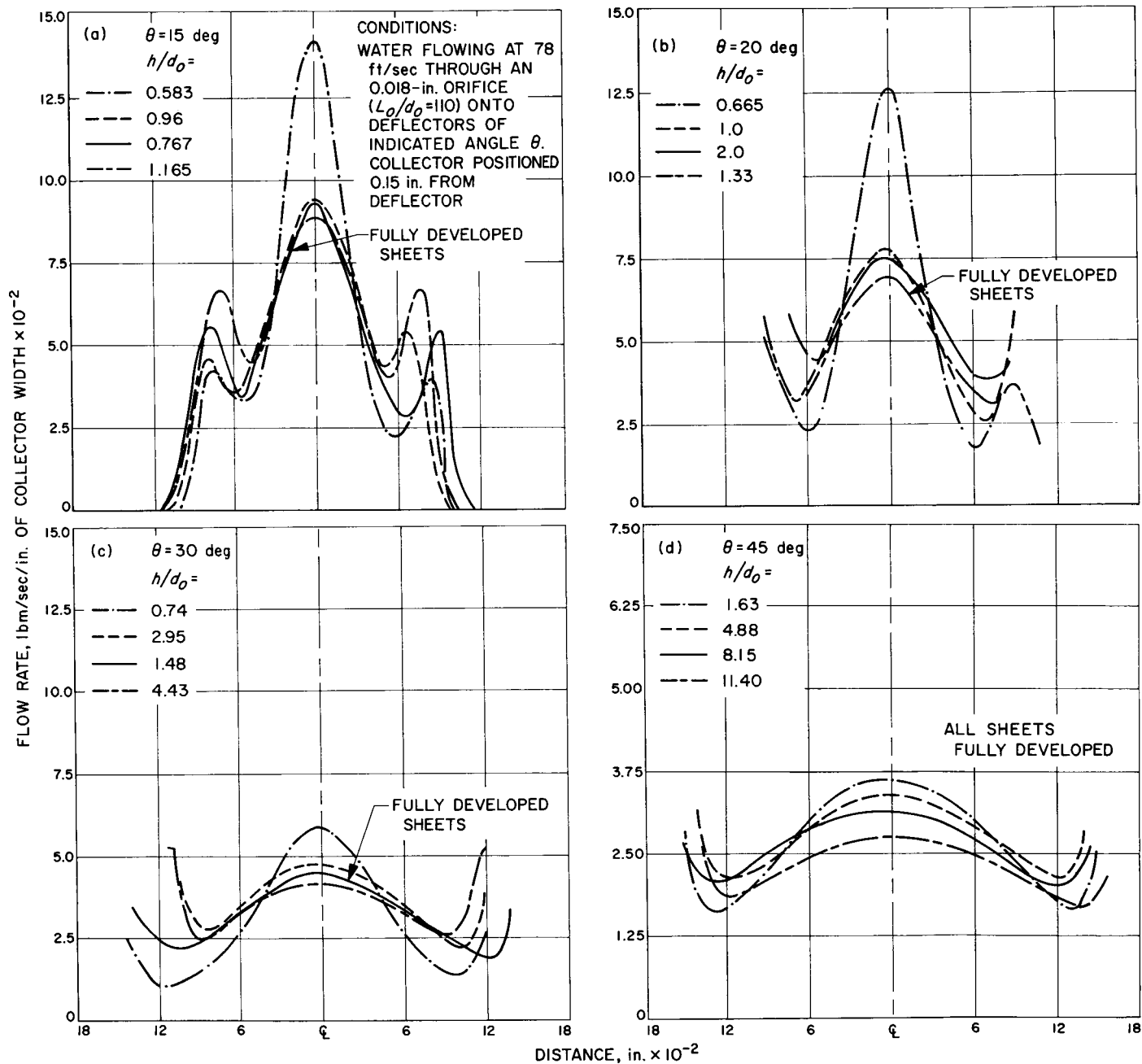*1. Mass flux distribution.* Numerous mass flux distribution curves were obtained, of which those presented in Fig. 17 are quite typical. To show all the curves clearly, Fig. 17 has been divided into four parts, (a) through (d), according to the deflector angle θ of the sheet-formation device. In general, the mass flow rate is distributed symmetrically about the sheet centerline and has a sharp, central peak with a well-defined maximum. The bell-shape is altered (to a greater or lesser degree, depending on the specific deflector geometry) only by two small side peaks coinciding with the edge ribs noted during the photographic study. When these ribs are taken into account, integration of any distribution curve gives approximately the total mass flow rate issuing from the orifice, as would be expected.

Examination of Fig. 17 reveals that the curves for θ's of 15, 20, and 30 deg fall into two distinct groups, depending on h/d_0. For example, in Fig. 17(a), the central portions of three of the mass flow distribution curves are essentially coincident, while one stands off by itself. Similar observations can be made for curves in Figs. 17(b) and 17(c). In each of these cases, the coincident curves are for deflectors with an overhang ratio $h/d_0 > 0.75$ (Category B) while the "different" curve is for a deflector with $h/d_0 < 0.75$ (Category A). Neglecting the end effects, the well-collimated mass flow-rate profiles for each Category A stream resemble those in a round jet much more than do those for the Category B streams. Based on the photographic evidence cited earlier, the latter have been designated as "fully-developed sheets" in Fig. 17.

It was subsequently discovered that the many individual distributions could all be condensed into a few completely general curves which correlated the data for all sheets, regardless of injection velocity, fluid physical properties, or the scale of the apparatus. This was accomplished by normalizing both $d\dot{w}/dx$ and the corresponding distance x across the sheets (measured outward from the centerline) into appropriate dimensionless ratios. The mass flux per unit width of sheet, $d\dot{w}/dx$, was normalized by dividing it by the fluid density, fluid velocity, and orifice diameter to obtain a dimensionless "mass distribution parameter,"

$$\mathcal{W}\left(\frac{x}{d_0}\right) \equiv \frac{d\dot{w}}{dx} \cdot \frac{144}{\rho \overline{V} d_0} \tag{10}$$

The distance x across the sheet was normalized by dividing it by the orifice diameter d_0.

Some typical normalized mass distribution data are plotted in Fig. 18 for Category B sheets. Included on each plot is the overall sheet width-to-diameter ratio w/d_0 at the edge of the deflector. The maximum values of x/d_0 for the distributions of Fig. 18 are greater than the corresponding w/d_0 values because the distribution data were taken 0.15-in. away from the edges of the deflectors. Even in that short distance, the sheets had spread considerably.

Fig. 18a was prepared from data obtained for sheets formed under widely varying conditions of geometry, Reynolds number, and Weber number. The only thing the six normalized mass distributions plotted in Fig. 18a had in common was their formation by deflector–orifice combinations with an overhang ratio h/d_0 of unity. Similar remarks apply to the plots of Fig. 18(b) and 18(c), which correlate data from sheets formed by deflectors with h/d_0 values of 2 and 3, respectively. Figure 18(b) includes data for one of the "large" deflectors, more than twenty times the size of the others. These results indicate that the distribution of mass flux across a sheet, when appropriate nondimensionalized, is nearly independent of injection velocity, fluid physical properties, and the scale of the apparatus. The normalized distributions appear to depend primarily on h/d_0, although for $1 \leq h/d_0 \leq 3$, even this dependency is slight.

2. Velocity distribution. A large number of velocity distribution curves was derived from the dynamic pressure measurements, as exemplified by the profile shown in Fig. 19. It was again found, however, that all the different velocity curves could be combined into a few correlations by normalizing both V_e and x. The fluid velocity V_e at each point across the width of the sheet was normalized by dividing it by the average exit velocity of the jet from which is was formed, to obtain a dimensionless "velocity distribution parameter,"

$$\mathcal{V}\left(\frac{x}{d_0}\right) \equiv \frac{V_e}{\overline{V}} \tag{11}$$

The distance x, as before, was converted to x/d_0.

Some typical normalized velocity distribution data are presented in Fig. 20. These results indicate that, like the distribution of mass flux, the sheet velocity distribution, when suitably nondimensionalized, is essentially independent of injection velocity and fluid physical properties. The normalized distributions again seem to depend mainly on h/d_0.
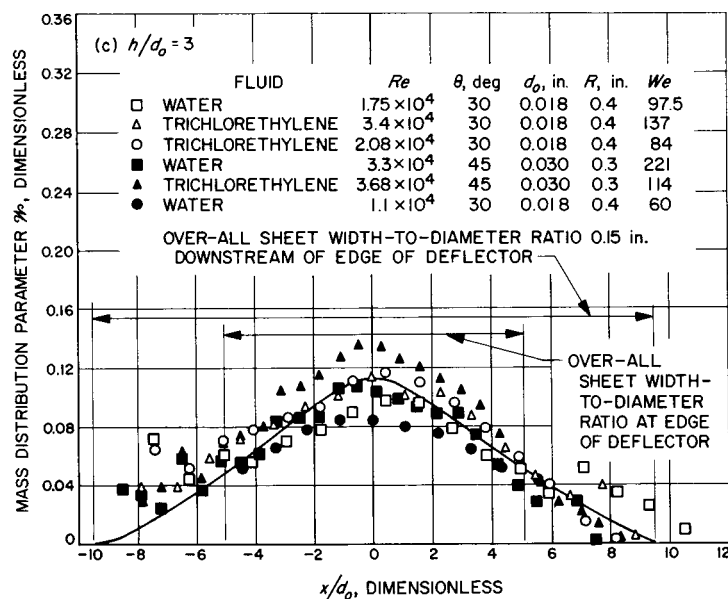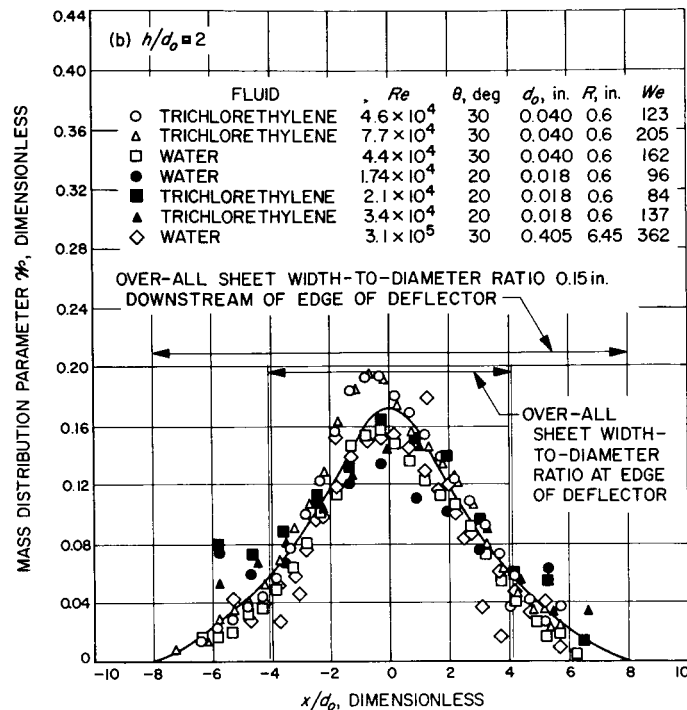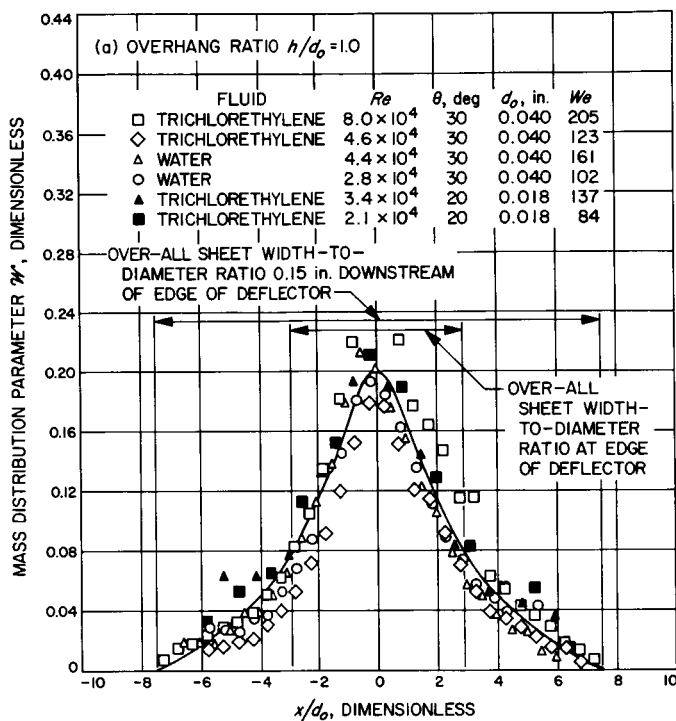
Fig. 18. Generalized mass flow-rate distribution in sheets formed on deflectors with several different overhang ratios at a station 0.15″ downstream of edge of deflector
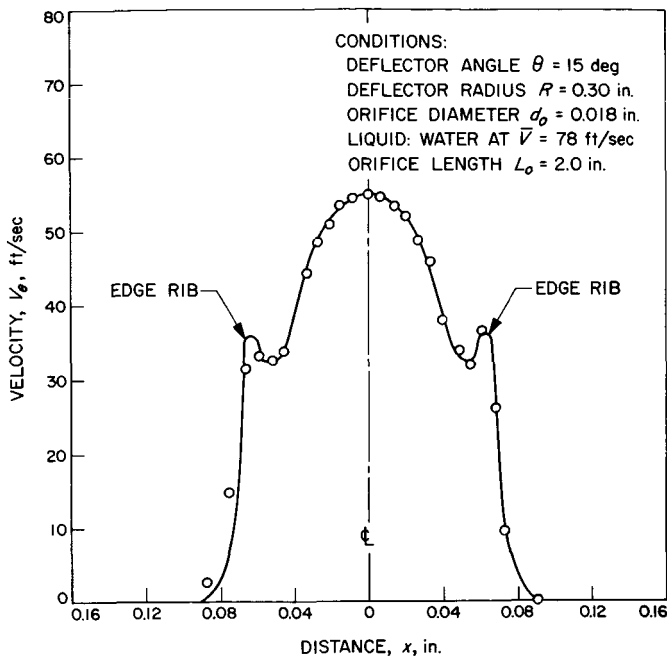
Fig. 19. Typical velocity profile across a free-flowing sheet at a station 0.15" downstream of edge of deflector
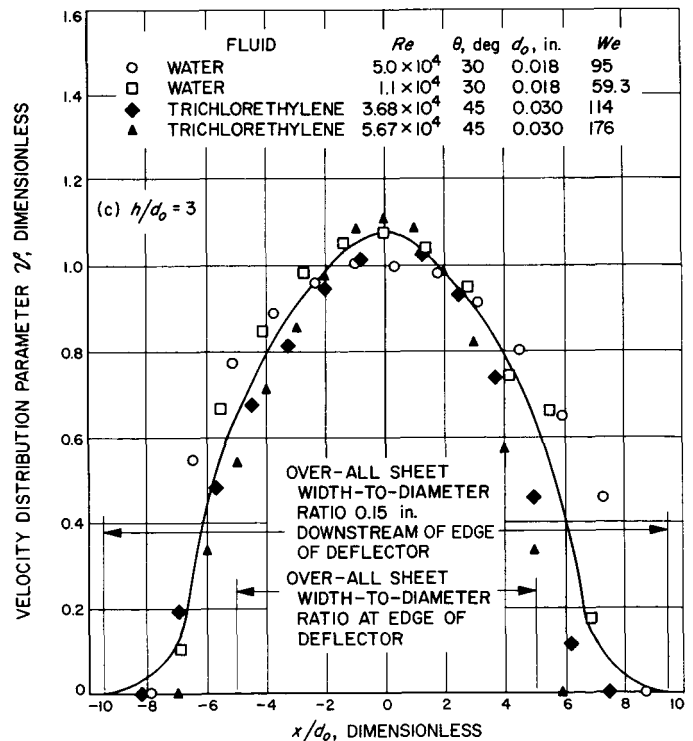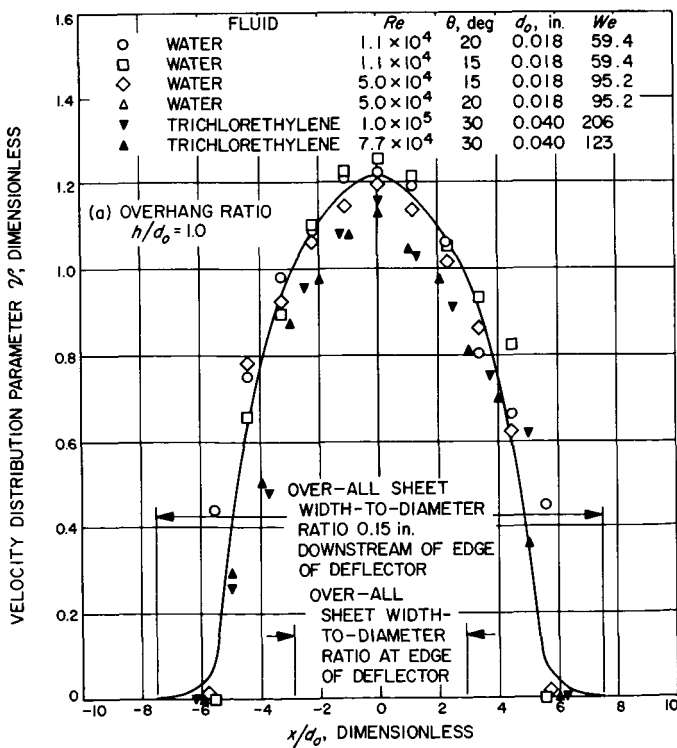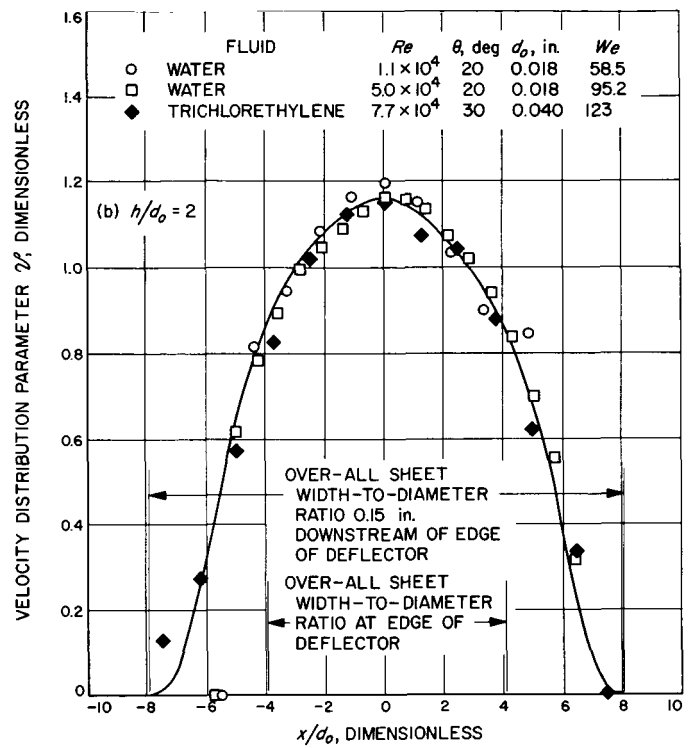
Fig. 20. Dimensionless velocity distribution curves for deflectors with several different overhang ratios at a station 0.15" downstream of edge of deflector

It is not practical to present here the many velocity distribution curves derived from the experimental measurements. However, the effect on these distributions of increasing the overhang ratio is to make them broader and flatter. The manner in which $\mathcal{Q}'$ decreases with h/d_0 may be seen in a simplified fashion by examining the variation of only one point (the value of $\mathcal{Q}'$ at the sheet centerline) on each curve. This is plotted in Fig. 21.

The data shown on Fig. 21 plots as a straight line on semilogarithmic coordinates. It is presented here on full logarithmic coordinates so that an anomalous cusp, which occurs in the vicinity of $h/d_0 = 0.75$, may be seen in greater detail. There were only a limited number of experimental deflectors with $0.6 \lesssim h/d_0 \lesssim 0.9$, but for each of these the dynamic pressures measured at the sheet centerline, and the corresponding values of $\mathcal{Q}'$, were considerably lower than those obtained outside that h/d_0 range.

D. Distributions Derived From Mass and Velocity Data

1. Thickness distribution. It is extremely difficult to measure sheet thickness accurately, even for sheets

formed on the "large" (6.45-in. radius) deflectors, because the sheets are extremely thin (typically about 0.005 in. thick). However, the generalized mass and velocity distribution curves may be used to *estimate* correspondingly general sheet thickness distribution curves. Defining a "normalized sheet thickness" as

$$\mathcal{I}\left(\frac{x}{d_0}\right) \equiv \frac{t}{d_0} \tag{12}$$

it can be shown from the Continuity Principle that, at constant x/d_0 and h/d_0,

$$\mathcal{I} = \frac{\mathcal{Q}'}{\mathcal{Q}'} \tag{13}$$

Generalized thickness distributions calculated from the general mass and velocity curves of Figs. 18 and 20 are shown in Fig. 22, where the increased thickness characteristic of the edge ribs may be seen. The curve for $h/d_0 = 1$, for example, was obtained by dividing the curve of Fig. 18a by that of Fig. 20(a) point by point.

	FLUID	θ, deg	d_0, in.	Re	We
O	WATER	15	0.04	5×10^4	95
O	WATER	20	0.04	5×10^4	95
□	WATER	30	0.04	5×10^4	95
△	WATER	45	0.04	5×10^4	95
●	TRICHLORETHYLENE	15	0.04	7.7×10^4	123
●	TRICHLORETHYLENE	20	0.04	7.7×10^4	123
■	TRICHLORETHYLENE	30	0.04	7.7×10^4	123
▲	TRICHLORETHYLENE	45	0.04	7.7×10^4	123
◑	WATER	15	0.018	1.1×10^4	59.3
◑	WATER	20	0.018	1.1×10^4	59.3
◧	WATER	30	0.018	1.1×10^4	59.3
▲	WATER	45	0.018	1.1×10^4	59.3

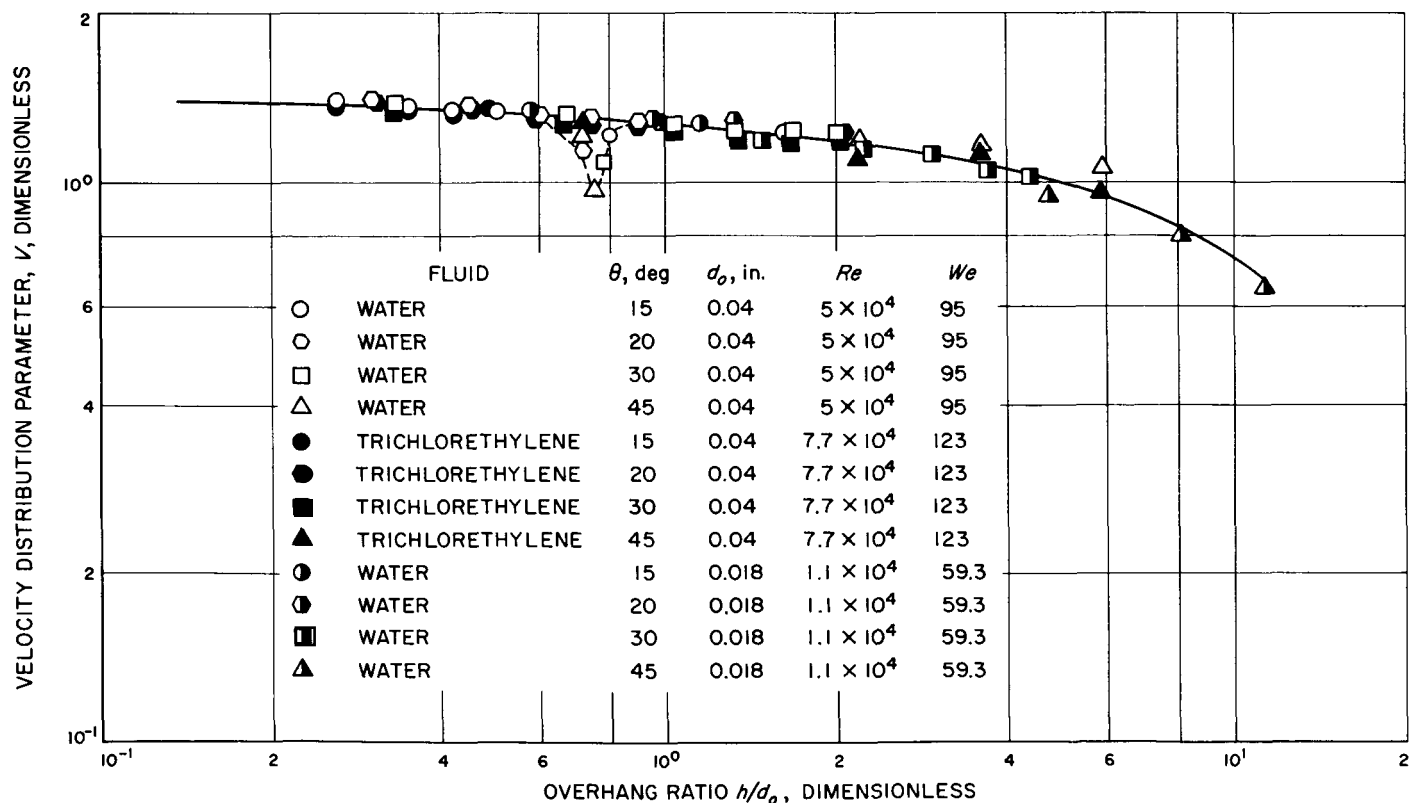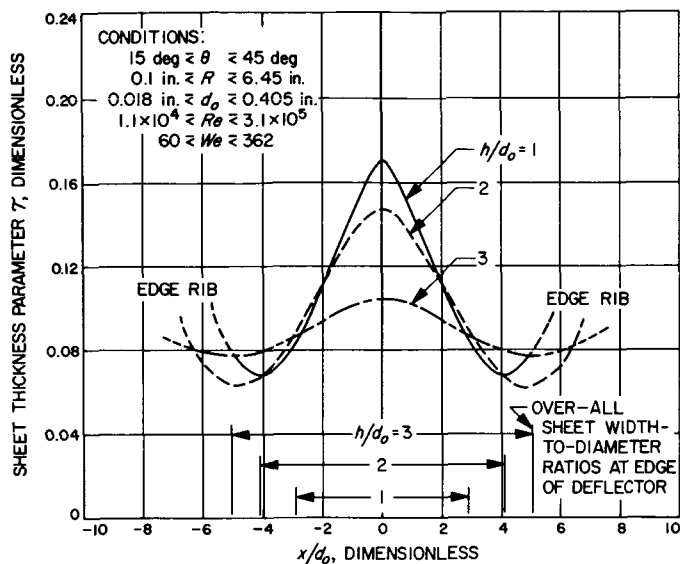**Fig. 21. Effect of deflector overhang ratio on normalized centerline velocity at deflector exit**

Fig. 22. Generalized thickness distributions for sheets formed on deflectors with several different overhang ratios at a station 0.15″ downstream of edge of deflector

Since these curves were derived from measurements taken 0.15 in. from the edge of the deflectors, they apply strictly only at that distance from the deflector exits. Visual observation indicates that the thickness of the free sheets appears to remain quite constant, though. To use Fig. 18 for a specific deflector, it is only necessary to multiply both abscissa and ordinate of the curve for the proper h/d_0 value by the orifice diameter. Actual sheet thickness vs actual distance across the sheet is then obtained.

The central curve $h/d_0 = 2$ was used to predict the thickness distribution for one of the large deflectors with that overhang ratio. The thickness in the actual flowing sheet (water, $\overline{V} = 100$ ft/sec) was then "measured" in a crude manner by inserting a machinist's rule. The predicted and measured values are compared in Table 2. Ranges, rather than discrete values, are given for the "measured" values to indicate the level of uncertainty. Nevertheless, agreement between the predicted and measured values was excellent across the whole sheet, illustrating the scalability of the generalized thickness distribution curves (derived from data collected for the "small" deflectors) to flow devices at least twenty times as large in linear dimension.

2. Momentum flux distribution. Similarly, the generalized mass and velocity distribution curves may be used

Table 2. Comparison of predicted and measured sheet thicknesses for large[a] deflector

Location	Predicted thickness, in.	Measured thickness, in.
Centerline	0.085	0.08 — 0.09
$\dfrac{x}{d_0} = 2$	0.063	0.05 — 0.06
$\dfrac{x}{d_0} = 4$	0.039	0.03 — 0.04

[a] $R = 6.45''$, $d_0 = 0.405''$, $\theta = 30$ deg, $\overline{V} = 100$ ft/sec, water.

to compute corresponding general momentum flux profiles across flowing sheets. Defining the stream momentum flux per unit sheet width at any point across the sheet as

$$M = \frac{d\dot{w}}{dx} \cdot V_e \qquad (14)$$

(at each discrete value of x/d_0), and incorporating Eqs. (10) and (11) results in

$$M = \frac{\rho \overline{V}^2 \, \mathcal{W} \, \mathcal{V} \, d_0}{144} \qquad (15)$$

M may then be normalized by dividing both sides of Eq. (15) by $\rho \overline{V}^2 \, d_0/144$ to obtain a dimensionless "sheet momentum flux parameter,"

$$\mathcal{M}\left(\frac{x}{d_0}\right) \equiv \mathcal{W} \, \mathcal{V}\left(\frac{x}{d_0}\right) \equiv \frac{144 \, M}{\rho \overline{V}^2 d_0} \qquad (16)$$

Equation (16) makes it convenient to calculate generalized momentum flux distributions from the previously-developed general mass and velocity curves. Typical plots covering the range of h/d_0 values of interest for injection devices are shown in Fig. 23. It is seen that for $1 \lesssim h/d_0 \lesssim 3$, a sheet's momentum flux is concentrated in its center, and falls off rapidly toward the edges. To obtain the absolute momentum flux profile for a particular flowing sheet, one would simply multiply the abscissae of the appropriate h/d_0 curve from Fig. 23 by d_0, and the ordinates by $\rho \overline{V}^2 d_0/144$.

E. Observation of Sheet Stability

The visual characteristics of flowing sheets were briefly investigated by means of high-speed cinematography.
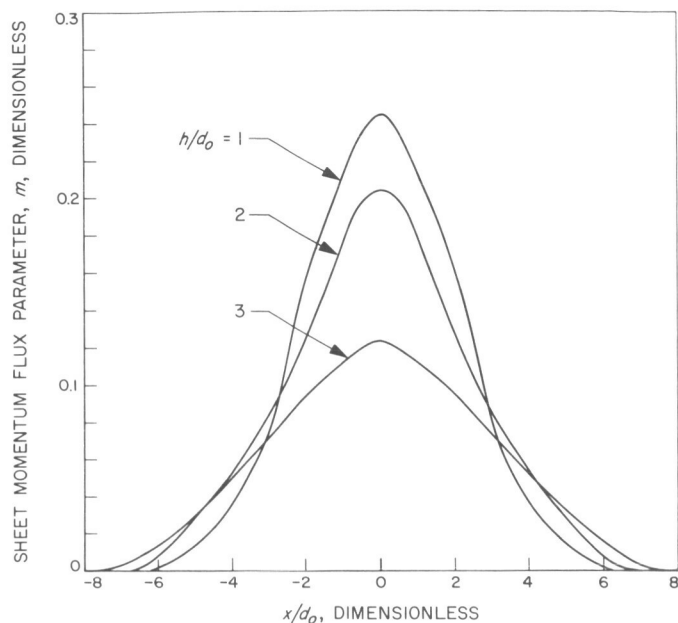
Fig. 23. Generalized momentum flux distributions for sheets formed on deflectors with several different overhang ratios at a station 0.15″ downstream of edge of deflector

Examination of successive frames of motion picture film indicated that the sheets were susceptible to two types of instability. The first was a random time-variation in the principal dimensions while the sheets were still being formed on the deflectors; this was influenced mainly by the orifice hydraulics. The second was a premature disintegration of the sheets after they had left the deflectors; the fluid physical properties appeared to exert the primary influence on that phenomenon.

In all cases where the shorter $[6 \lesssim (L_0/d_0) \lesssim 12]$ orifices were used, the sheet boundaries and therefore the width and spreading angle varied randomly ($\sim \pm 10\%$) with time. Frequently, the jets themselves were unstable. The appearance of a typical sheet of water formed from a short orifice is shown in Fig. 24(a); in the complete motion picture sequence, this sheet randomly "writhes" around on the deflector. When the experiments were repeated under identical conditions except for long ($L_0/d_0 = 100$) orifice tubes, the instability disappeared and no dimensional variations could be detected from frame to frame. The improvement in the visual properties of the sheet under these conditions is evident in Fig. 24(b).

The effect of orifice hydraulic environment was the most pronounced for sheets of Category A ($h/d_0 \lesssim 0.75$); for Category B ($h/d_0 \gtrsim 0.75$) it was less, although still

(a) ORIFICE LENGTH–TO–DIAMETER RATIO OF 10

(b) ORIFICE LENGTH–TO–DIAMETER RATIO OF 100
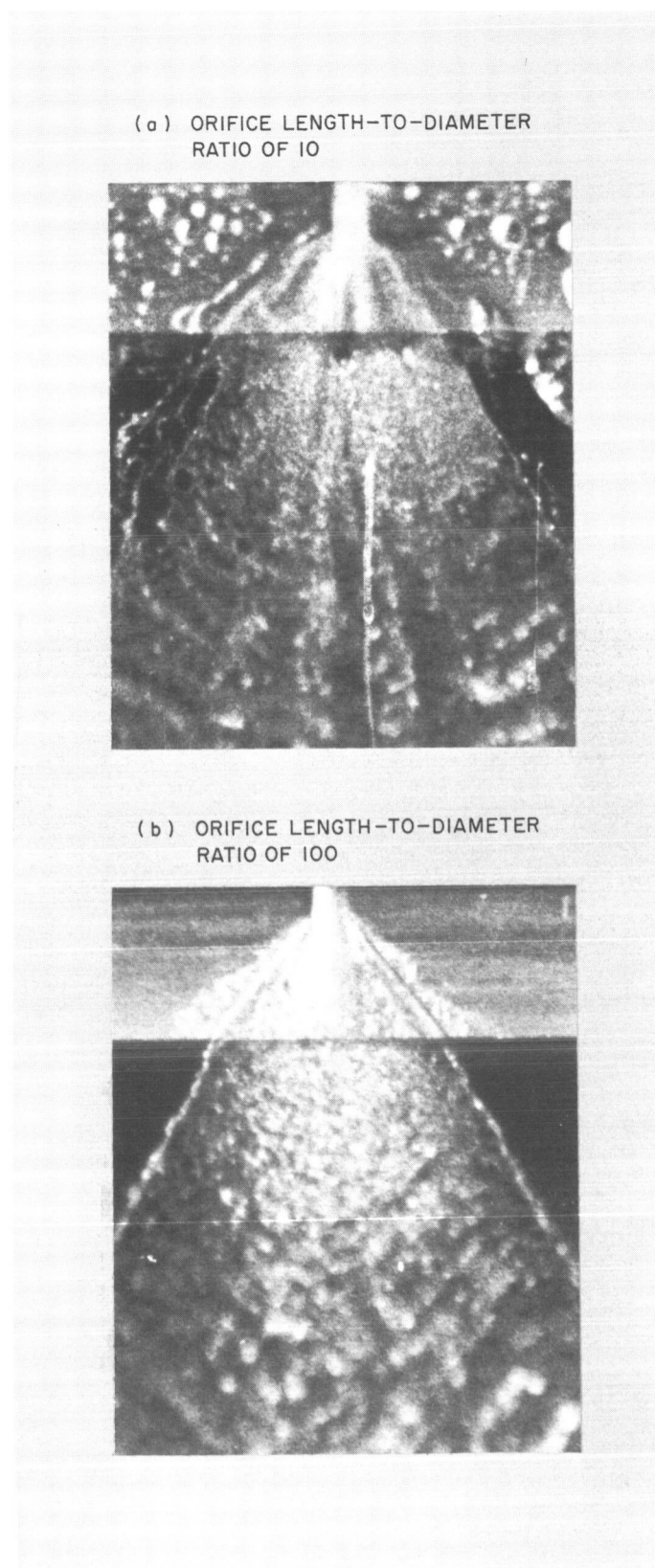
Fig. 24. Influence of orifice hydraulics on sheet stability

appreciable. For sheets formed on very long deflectors (Category C), the orifice length-to-diameter ratio did not exert a very large influence on sheet stability.

All sheets formed from water had appearances similar to the sheets of Fig. 7(a and b); sheet integrity was maintained for some distance past the injector. The n-hexane sheets disintegrated much more quickly, however. Figure 25 shows several successive views of flat sheets formed on 30-deg deflectors by n-hexane flowing at $\overline{V} = 80$ ft/sec. The time increment between frames in both rows is about 1.4 $\times$ 10⁻⁴ sec. The top sequence is for a deflector with an h/d_0 of 0.33; the bottom, for a deflector with $h/do_0 = 1.33$. In both cases, the sheets begin to break up immediately after leaving the deflector, and the resulting ligaments are released in a discontinuous, pulsating manner.

F. Effect of Surface Wettability

A single experiment was conducted to illustrate the effect of deflector surface wettability on sheet dimensions. Water was first introduced through a 0.018-in.-diameter
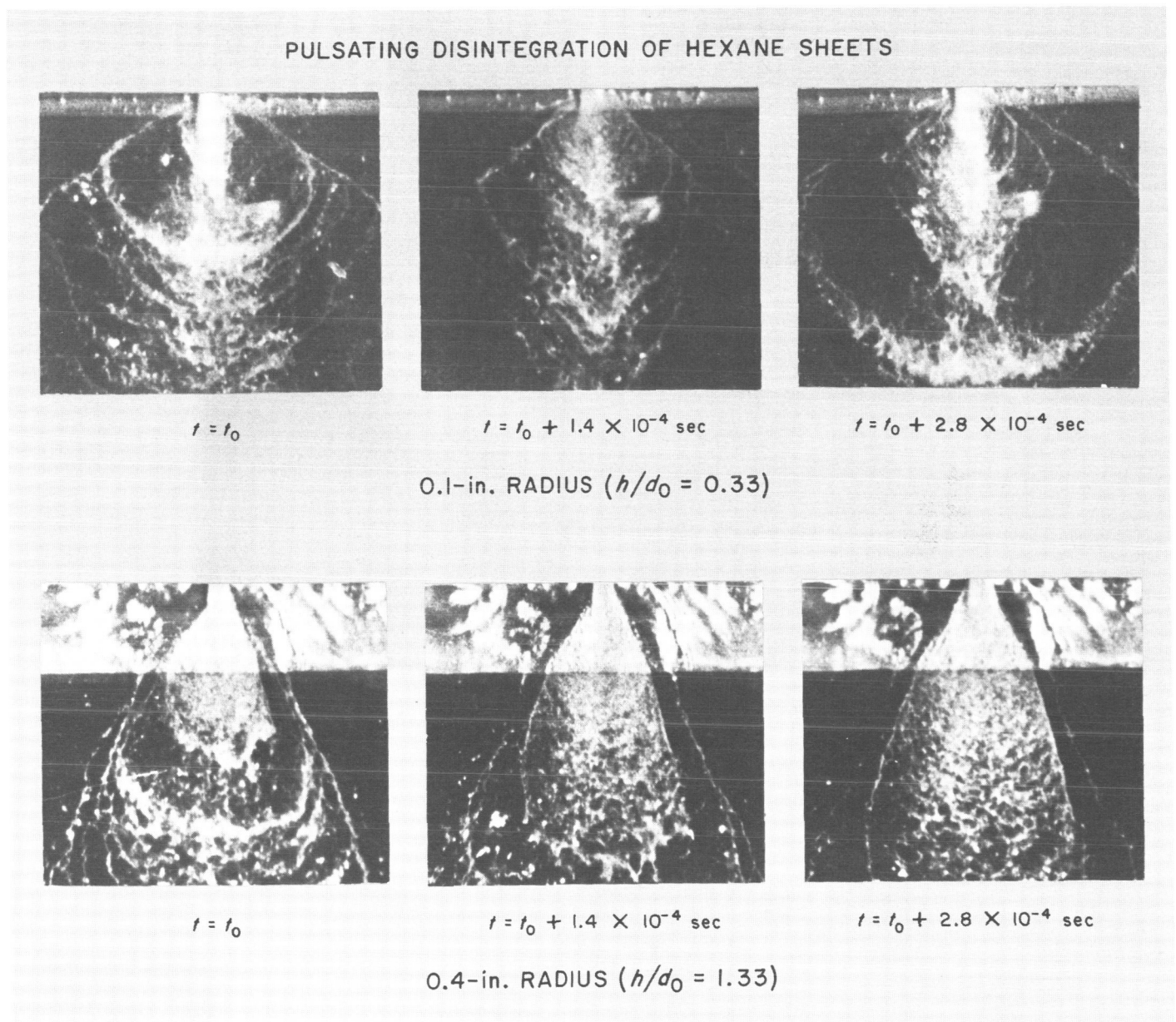
Fig. 25. Disintegration of pulsating hexane sheets
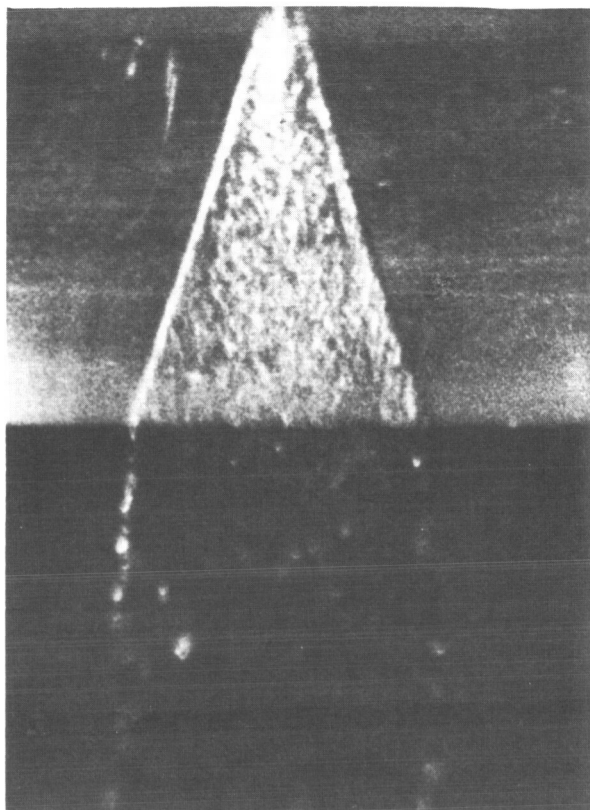
(a) SURFACE WET BY
LIQUID SHEET

(b) SURFACE NOT WET BY
LIQUID SHEET

Fig. 26. Effect of deflector surface wettability on sheet width

$(L_0/d_0 = 110)$ orifice tube at $\overline{V} = 100$ ft/sec onto a clean (degreased) aluminum deflector surface of 0.7-in. radius and 45-deg included angle. The resulting liquid sheet is shown in Fig. 26(a). Next, a thin, uniform coating of silicone grease was applied to the deflector surface, and water was introduced at the same velocity. The appearance of the corresponding sheet is shown in Fig. 26(b). The sheet width is clearly reduced when the liquid does not wet the surface. The width reduction was 25% in this instance. The spreading angle of the free sheet was, however, unaffected.

IV. Discussion of Results

A. Sheet Formation and Stability

The experimental results indicate that when round jets are tangentially introduced to cylindrical deflector surfaces, true sheets will not form unless the overhang ratio (h/d_0) of the device exceeds about 0.75. Below this critical

value, the effect of the deflector surface protruding into the jet is simply to perturb it in much the same manner that a tiny burr at the orifice exit would. Although most of the mass of the resultant stream remains concentrated in its jet-like central core, considerable splattering occurs, giving rise to the ragged or feathered appearance, and the ill-defined boundaries characteristic of Category A (Fig. 7).

A tiny burr protruding only a slight distance into a round jet will cause the jet to deflect through a very large angle. Likewise, a deflector surface protruding to a very small distance $(h/d_0 < 0.75)$ into the jet will deflect it through a similarly large (15 to 25 deg) angle, as shown in Fig. 16. Thus, the mechanism on deflectors with $h/d_0 \simeq 0.75$ appears to be one of jet perturbation, rather than sheet formation. Somewhere in the region around $h/d_0 = 0.75$ a transition to fully developed sheet flow (Category B) must occur. Both visual characteristics and the velocity curve of Fig. 21 point to a minimum h/d_0 of about 1 for good sheet formation.

The location of the transition region appears to be substantiated by the curious cusp of Fig. 21, which indicates a larger loss of stream energy between h/d_0 values of 0.6 and 0.9 than in either of the adjacent regions. Although a thorough study of the dynamics of the phenomena occurring within this limited region was well beyond the scope of the present investigation, it seems reasonable to regard the presence of this cusp as indicative of a transition between the two flow Categories A and B.

Moreover, the transition between perturbed jets and fully developed sheets depends mainly on the geometrical factor, h/d_0. Injection velocity $\overline{V}$ and the fluid physical properties have very little, if any, effect, as shown by Figs. 16 and 21, which are all-inclusive with regard to these variables.

For all deflectors with $h/d_0 > 0.75$, true sheets will always form. However, as the deflectors are made longer and longer, energy losses become appreciable. Surface effects begin to predominate and the sheets, although initially well formed, deteriorate rapidly, and may even have degenerated into separate streams by the time they leave the deflectors (Fig. 7d). It would seem, then, that there is no real transition between Categories B and C (in the sense that there is one between A and B). Instead, some arbitrary value h/d_0 can be chosen, above which the sheets dissipate too much energy on the deflectors to be useful in most injector applications. From both visual characteristics and the velocity curve of Fig. 21, the maximum allowable h/d_0 seems to be about 5.

Within this recommended operating envelope $(1 \lesssim h/d_0 \lesssim 5)$, the use of low overhang ratios is desirable to minimize energy losses on the deflectors. On the other hand, the maximum (centerline) sheet thickness *decreases* as h/d_0 increases, as shown in Fig. 22. There may very well be some injector applications where the optimum value of h/d_0 would result from trade-offs between sheet thickness and energy utilization considerations.

The existence of randomly-varying propellant sheet properties can make complete description and control of the injection (and, thus, the combustion) process difficult, if not impossible. The sheet stability results showed that the key sheet dimensions can vary randomly with time about their mean values, and that liquid can be released discontinuously from the deflectors, if care has not been taken to assure controlled, reproducible hydraulics in the manifold and orifice entrance. Ideally,

zero manifold cross-flow velocities and very gradual, carefully-contoured transitions between the manifold and the orifice flow areas should be used. However, these conditions are often relaxed in production injectors to reduce manufacturing complexity. The resulting high manifold velocities and sudden flow area transition conditions will usually introduce flow irregularities at the entrance to an orifice, which can lead to various jet instabilities if the orifice is not long enough to damp them out. When such unstable jets are spread out into thin sheets, the randomly-fluctuating disturbances in the jet are magnified, giving rise to unstable sheets like that of Fig. 24(a). It has been shown (Ref. 6) that time-varying flow perturbations stemming from poor manifold or orifice entry design can be smoothed enough to effectively eliminate jet (and therefore sheet) instabilities if the flow regime at the orifice exit is fully developed turbulent.

The simplest way of assuring the fully-developed turbulent flow necessary to the full prediction and control of propellant sheet formation is the use of long $(L_0/d_0 \gtrsim 50)$ orifices. However, turbulence-inducing sections near the entrance produce equivalent degrees of developed turbulance in much shorter orifice passages (Ref. 6).

B. Sheet Dimensions and Orientation

The dimensionless sheet width (w/d_0), spreading angle (β) and deflection angle (δ) were found to be essentially independent of the liquids employed and the physical size of the sheet-formation device. A second-order injection velocity effect was noted for w/d_0 and β, but deflector geometry $(R, d_0,$ and $\theta)$ exerted the primary influence on sheet dimensions and orientation.

This may initially seem surprising, since, from dimensional considerations, it would be expected that these sheet properties should be functions of the velocity and liquid properties, as well as of geometric factors. Thus, if gravity and air-drag effects are dismissed as negligible for the regions of interest, we would have,

$$w = f_1[R, d_0, \theta, \overline{V}, \rho, \mu, \sigma] \qquad (17)$$

or, by dimensional analysis of these pertinent parameters,

$$\frac{w}{d_0} = f_2\left[\frac{R}{d_0}, \theta, Re, We\right] \qquad (18)$$

Similar expressions would be expected to hold for all geometrical properties of the sheet, e.g.,

$$\beta = f\left[\frac{R}{d_0}, \theta, Re, We\right] \qquad (19)$$

$$\delta = f\left[\frac{R}{d_0}, \theta, Re, We\right] \qquad (20)$$

However, the Reynolds number (Re) and Weber number (We) effects are slight over the regions of interest. This is illustrated in Figs. 27 and 28, where the geometrical parameters of the sheet are plotted against Re and We, respectively, for several typical fixed values of hardware geometry (θ and R/d_0).

Unfortunately, it is not possible to hold We constant for some fixed deflector geometry while systematically varying Re, or vice versa. A change in We can only be made by varying velocity, physical properties, or geometry, any of which variations will bring about a corresponding change in Re. However, it may be inferred from the plots of Figs. 27 and 28 that the near invariance of the sheet dimensions with Re and We accounts for the observed second-order influence of fluid velocity and physical properties. Thus, in the region of interest, which is defined as follows:

$$\left\{\begin{array}{c} 2 \lesssim \dfrac{R}{d_0} \lesssim 40 \\[2mm] 15 \lesssim \theta, \deg \lesssim 45 \\[2mm] 10^4 \lesssim Re \lesssim 10^5 \\[2mm] 50 \lesssim We \lesssim 10^3 \end{array}\right\}$$

we have nearly complete geometrical similarity, allowing functional relationships such as Eq. (18) to be very greatly simplified from a four-parameter to a two-parameter dependence; i.e.,

$$\frac{w}{d_0} \cong f_1\left[\frac{R}{d_0}, \theta\right] \qquad (21)$$

$$\beta \cong f_2\left[\frac{R}{d_0}, \theta\right] \qquad (22)$$

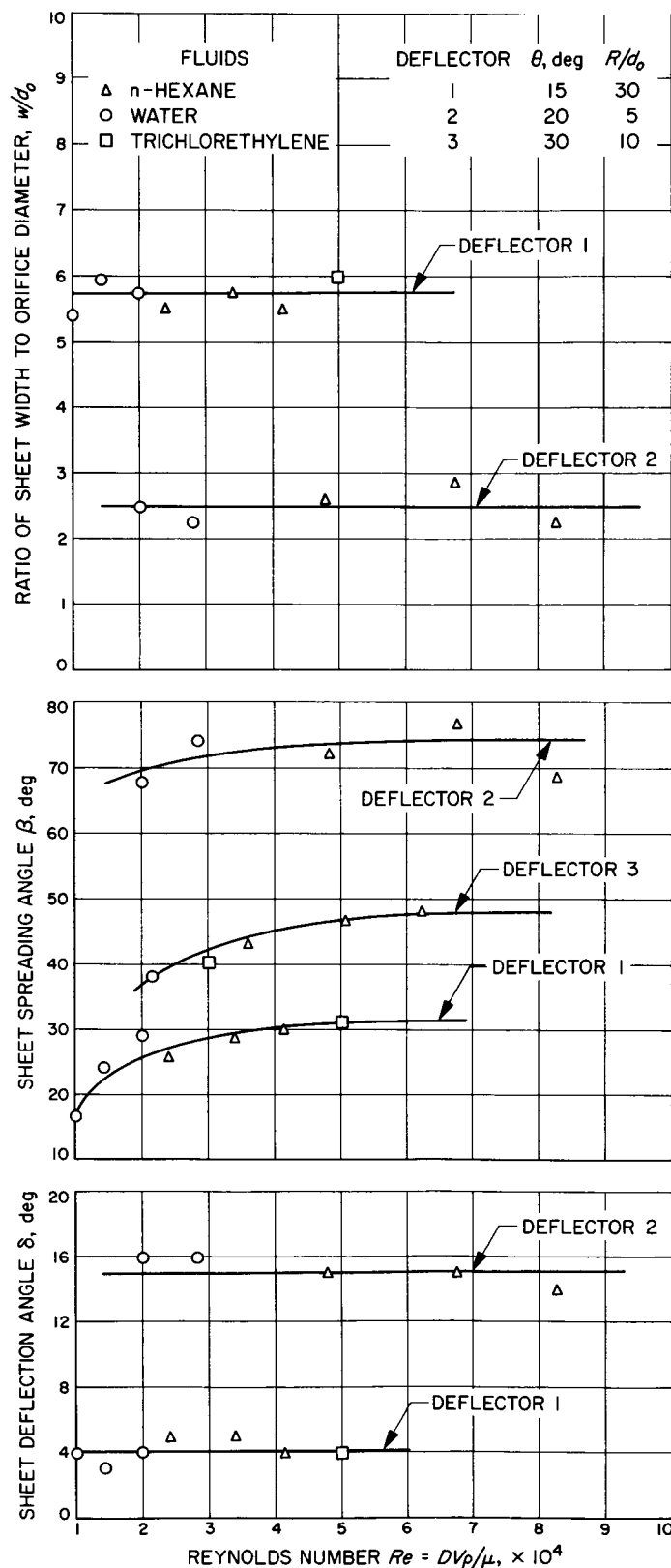$$\delta \cong f_3\left[\frac{R}{d_0}, \theta\right] \qquad (23)$$

Fig. 27. Effect of Reynolds number on sheet dimensions and orientation for typical deflector geometries
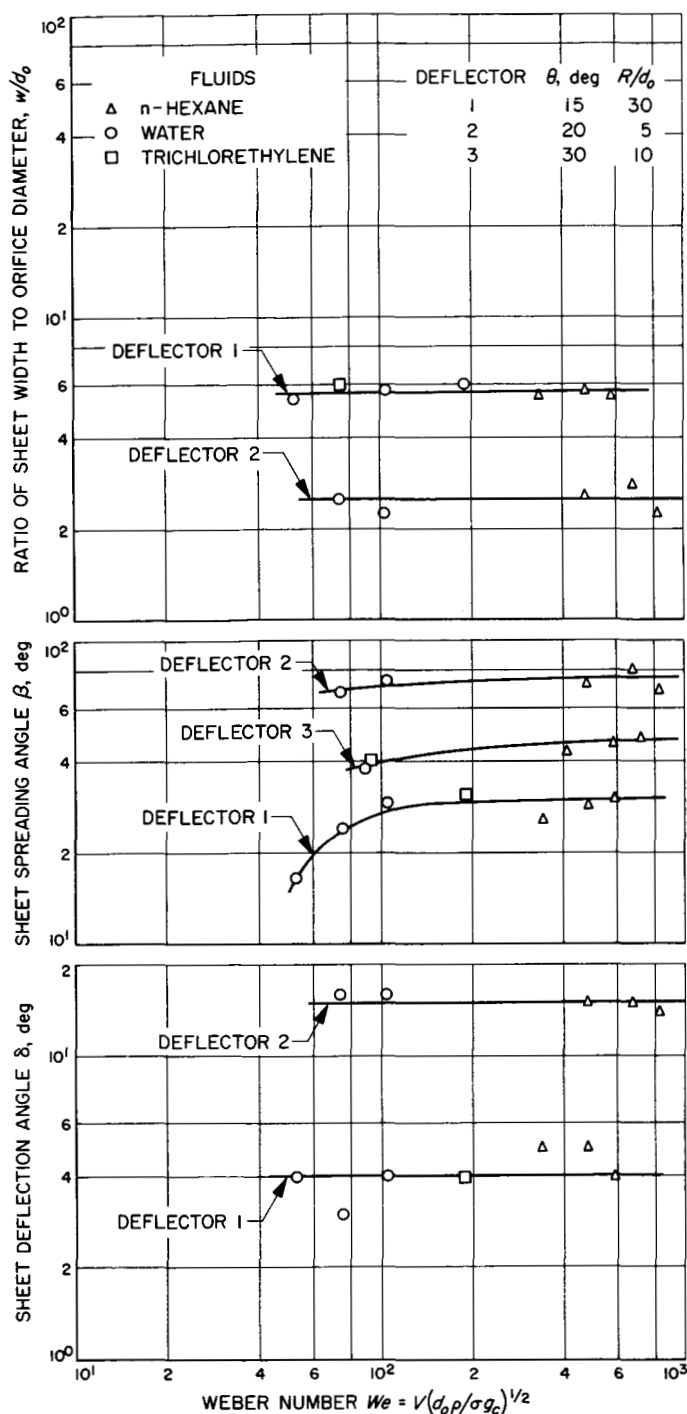
Fig. 28. Effect of Weber number on sheet dimensions and orientation for typical deflector geometries

Fig. 29. Sheet geometry on deflector (simplified)

the very weak dependence of β on σ and V (Eq. 8) is contrary to Eq. (22), the deviation is small.

It is interesting to note that the dependence of β on θ that is permissible by Eq. (22) is negligibly weak [θ is absent from the empirically determined Eq. (8)]. This is reasonable if one considers a crude model of the flowing sheet: assume the curved sheet to be flattened into a plane surface and to emanate from a point source (infinitely small orifice), as shown in Fig. 29. By inspection,

$$\tan\left(\frac{\beta}{2}\right) = \frac{w}{2L} \tag{24}$$

where the deflector arc length

$$L = \frac{\theta \pi R}{180} \tag{25}$$

Substituting Eqs. (4) and (25) in Eq. (24) gives

$$\tan\left(\frac{\beta}{2}\right) = \frac{k(1 - \cos\theta)^{1/2}}{\theta \left(\dfrac{R}{d_0}\right)^{1/2}} \tag{26}$$

The empirically determined Eq. (4) is consistent with the functional dependence of Eq. (21). In addition, the results presented in Fig. 16, which show δ as a function of h/d_0, are in agreement with Eq. (23). Finally, although

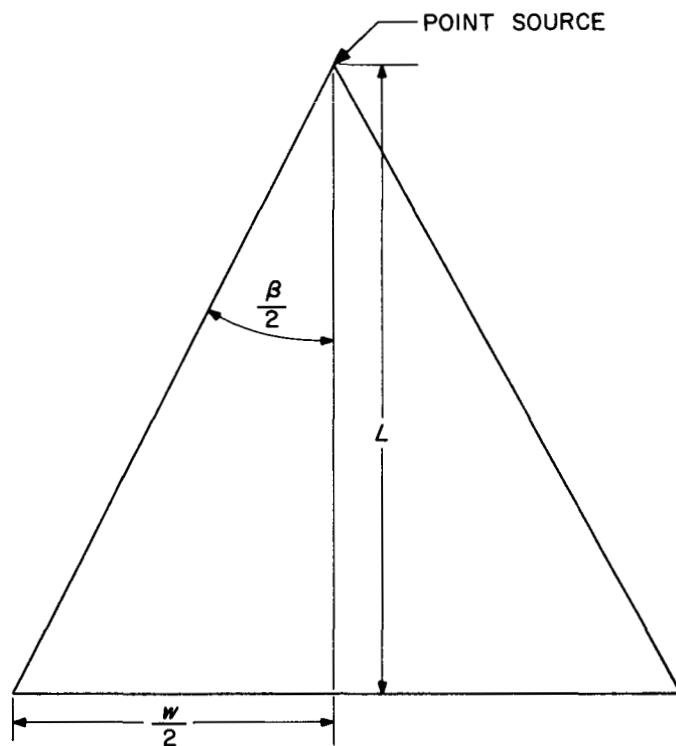Equation (26) contains R/d_0 and θ, and is therefore of the general form of Eq. (22). However, the term $(1-\cos\theta)^{1/2}/\theta$ has the unique property of being essentially constant for $0 < \theta, \text{deg} < 45$. Accordingly, Eq. (26) simplifies to

$$\tan\left(\frac{\beta}{2}\right) \cong \frac{k'}{\left(\dfrac{R}{d_0}\right)^{1/2}} \qquad (27)$$

This is similar to the empirically found relationship of Eq. (8) in that $\beta \cong f(R/d_0)$ only. Plotting $\tan(\beta/2)$ versus R/d_0 shows the correct data trend, but, because of the simplifying assumptions involved, Eq. (27) does not correlate the experimental data as well as the empirically determined Eq. (8) or its simplified version Eq. (9).

C. Sheet Mass and Velocity Distributions

From dimensional considerations, it would be expected that $\mathcal{W}$ should be a function of the velocity and liquid properties, as well as of geometric factors:

$$\mathcal{W} = f\left[\frac{x}{d_0}, \frac{R}{d_0}, \theta, Re, We\right] \qquad (28)$$

However, if and only if Reynolds number (Re) and Weber number (We) effects were negligible over the ranges of variables studied, as was found to be the case for the sheet dimensions, Eq. (28) would reduce to

$$\mathcal{W} \cong f_1\left[\frac{x}{d_0}, \frac{R}{d_0}, \theta\right] \qquad (29)$$

Since some of the sheet dimensions were earlier found to be best correlated with the overhang ratio (h/d_0), it would not be surprising if the mass flux distribution might also depend on h/d_0 as well as on x/d_0. Then, substitution of

$$\frac{h}{d_0} = \frac{R}{d_0}(1 - \cos\theta) \qquad (30)$$

into Eq. (29) would give the experimentally-observed relation,

$$\mathcal{W} \cong f_2\left[\frac{x}{d_0}, \frac{h}{d_0}\right], \qquad (31)$$

a reduction from a five- to a two-parameter dependence.

Further, at constant h/d_0,

$$\mathcal{W} \cong f_3\left[\frac{x}{d_0}\right]_{\frac{h}{d_0}} \qquad (32)$$

Eq. (32) implies that, if Re and We effects are truly negligible, and if h/d_0 is a valid substitution for R/d_0 and θ in the functional relationship of Eq. (29), all deflectors with a constant value of h/d_0 will produce dynamically and geometrically similar sheets (regardless of the fluids, velocities, or physical sizes involved), whose mass distributions are given by a single curve in which $\mathcal{W}$ is plotted versus x/d_0. Varying h/d_0 would then be expected to produce a *family* of general mass flux distribution curves. This is exactly what was found experimentally (Fig. 18).

By reasoning similar to that employed in the analysis of mass flow rate distribution, it would be expected that

$$\mathcal{V} \cong f\left[\frac{x}{d_0}, \frac{h}{d_0}\right] \qquad (33)$$

if Reynolds and Weber number effects were again negligible and the geometrical dependencies are reducible. All velocity distributions at constant h/d_0 would then be correlated by a single curve of $\mathcal{V}$ versus x/d_0, much as the mass distributions were found to be, and varying h/d_0 would be expected to produce a corresponding family of general velocity distribution curves. This contention was also verified by the experimental results (Fig. 20).

Comparative measurements would have sufficed to check the validity of Eq. (33). However, since it was found convenient to use the velocity distribution data in the prediction of sheet thicknesses some remarks concerning the degree of confidence that can be placed in these velocity data are in order. In the first place, the capillary tube probe, although the smallest that could be practically used, had a diameter of the same order of magnitude as the sheet thicknesses probed. Thus a local "average," rather than a centerline, velocity was encountered by the probe at each station across the sheet. Also, if some secondary (recirculatory) flow occurred within the probe, the pressure measured might not have indicated the true "stagnation" value at all. Finally, it was assumed that the velocity was related to the dynamic pressure by Eq. (2), a customary definition of velocity head.

There were no "primary standards" against which to check the present data, because so far as is known, no previous workers have ever measured velocities in such

exceedingly thin flowing sheets. The variation with free-stream distance of the centerline velocity in jets from round orifices has been studied, however. Rupe (Ref. 6) measured centerline stagnation pressure in 0.12-in.-diameter jets, using a so-called "flat-plate probe" (a flat plate with a hole in it, against which the jets impinged perpendicularly), believed to have some advantages over the more conventional Pitot tube approach used in the present experiments. As a check then, the variation with free-stream distance of the centerline velocity in several jets from the small (0.018 to 0.040-in.-diameter) orifices used in the present studies was measured with the capillary tube probe, and the results compared (Fig. 30) with those of Rupe.
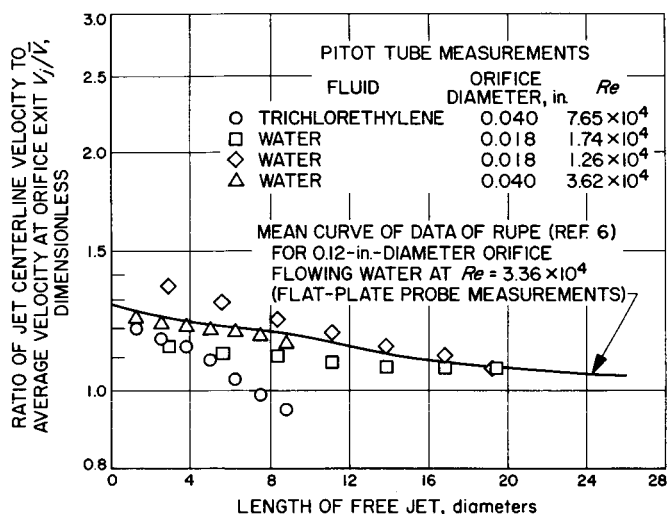

Fig. 30. Comparison of normalized jet centerline velocities measured by two alternative methods

Figure 30 shows a fair comparison between Rupe's flat-plate data and the author's Pitot tube results in the region from 3.75 to 7.5 jet diameters downstream of the orifice (where sheet velocities were measured). The amount of scatter from one set of conditions to the next indicates a difference of perhaps ±10% between the capillary tube measurements and *Rupe's* data. However, it is still not possible to assign absolute values of experimental accuracy due to the uncertainties in *Rupe's* results. The fact that Rupe was unable to reproduce, with the flat-plate probe measurements, either the uniform velocity profile of LeClerc (Ref. 7) or the Prandtl centerline stagnation pressure for fully developed turbulent pipe flow (Ref. 8), shows just how difficult accurate measurements of this sort really are. Nevertheless, the comparison between measured and predicted sheet thickness (Table 2) sub-

stantially increases the confidence level of the velocity distribution data from which the thickness curves were derived.

D. Thickness and Momentum Flux

Since by Eqs. (13) and (16) $\mathcal{I}$ and $\mathcal{M}$ are just functions of $\mathcal{W}$ and $\mathcal{V}$, relations similar to those for $\mathcal{W}$ and $\mathcal{V}$ would be expected to apply for $\mathcal{I}$ and $\mathcal{M}$:

$$\mathcal{I} \cong f\left[\frac{x}{d_0}, \frac{h}{d_0}\right] \tag{34}$$

$$\mathcal{M} \cong f\left[\frac{x}{d_0}, \frac{h}{d_0}\right] \tag{35}$$

This is borne out by the plots of Figs. 22 and 23.

V. Summary of Results

The experimental results may be summarized as follows:

1. The deflector overhang ratio (h/d_0) must be greater than 0.75 for true sheets to form; below this critical value, perturbed round jets with ill-defined properties are formed. As h/d_0 is increased above 1, however, energy dissipation due to frictional losses on the deflectors also increases, so that $h/d_0 = 3$ would seem a reasonable upper limit for practical sheet-formation devices. On the other hand, maximum sheet thickness *decreases* as h/d_0 becomes larger, and there may be some applications where the "optimum" value of h/d_0 would result from trade-offs between thickness and energy utilization considerations.

2. The sheet dimensions, such as normalized width (w/d_0), spreading angle (β) and deflection angle (δ), are all virtually independent of fluid physical properties, injection velocity, or actual size of the flow device, over the range $10^4 \lesssim Re \lesssim 3 \times 10^5$. They vary with, and may be correlated in terms of, simple dimensionless geometrical ratios. Sheets formed by the tangential impingement of round jets on concave, cylindrical deflector surfaces exhibit nearly complete *dynamic* and *geometric similarity*, thus permitting accurate prediction, control, and scaling of the key sheet properties.

3. Upstream hydraulic conditions have no apparent effect on the time averaged properties of flowing sheets. But fully developed turbulent flow (orifice L_0/d_0's of 50 or greater) is necessary to produce stable sheets whose properties do not vary randomly with time about the average values.

4. The sheet properties are affected by the wettability of the deflector surfaces on which they are formed. The results of the present program were obtained with clean, degreased surfaces. Limited experimentation showed, however, that controlled application of coatings not wet by the fluid to the deflector surfaces could significantly alter some sheet properties.

5. The actual distributions of mass flux, velocity, thickness and momentum flux across the sheets depend upon fluid physical properties, injection velocity, and the scale of the apparatus. However, these may be *normalized* (expressed in terms of certain dimensionless ratios) to yield general correlations which depend only on the dimensionless overhang ratio, h/d_0.

VI. Concluding Remarks

Sufficient engineering information on the formation and properties of flowing sheets is now available to permit their intelligent application to a wide variety of injection and flow devices. Knowledge of the manner in which geometry influences sheet dimensions and spatial orientation permits the designer to select a deflector/orifice combination to produce sheets in a wide variety of configurations and direct them as required. Regions in which sheets unsuitable for use in rocket engine applications (because of excessive energy dissipation) are formed can

be avoided, and the sheet-formation apparatus can be tailored to produce the desired distributions of mass flow, velocity, momentum or thickness across the sheets. Criteria for achieving stable sheets (those with time-invariant properties) are also known. Methods for dimensionally matching impinging sheets from dissimilar deflectors have been developed. (Ref. 9)

If the assumption is made that momentum level does not exert an appreciable effect on the efficiency of mixing or atomization of a pair of unlike impinging sheets, the near invariance of sheet properties with injection velocity implies that an impinging-sheet injection element could be widely pressure throttled at constant mixture ratio with little or no change in combustion efficiency. This has, in fact, been accomplished (Refs. 10 and 11). The same results could be predicted for a showerhead-type device, such as the cup-and-plug element (Ref. 5) without that assumption.

The foregoing attractive possibilities, the very promising experimental results reported in Refs. 4, 10 and 11, and the scalability of the present results because of dynamic similarity, indicate that sheets formed as described herein are a versatile, flexible addition to injection technology. Their key properties are now subject to essentially complete prediction and control.

Nomenclature

English

d_0 orifice diameter, in.

g_c gravitational constant, $32.174 \dfrac{\text{ft lbm}}{\text{lbf sec}^2}$

h deflector overhang, in.; $h = R (1 - \cos \theta)$

L_0 orifice length, in.

$\mathcal{M}$ momentum distribution parameter, dimensionless;

$$\mathcal{M} \equiv \frac{q v d^2}{\mathcal{I}}$$

P_d dynamic pressure, $\dfrac{\text{lbf}}{\text{ft}^2}$

Re Reynolds number, dimensionless; $Re \equiv \dfrac{d_0 \overline{V} \rho}{\mu(144)}$

R deflector radius, in. (Fig. 1)

t sheet thickness, in.

$\mathcal{I}$ sheet thickness parameter, dimensionless;

$$\mathcal{I} \equiv \frac{q v}{q r}$$

Nomenclature (contd)

$\mathcal{V}$ velocity distribution parameter, dimensionless;
$$\mathcal{V} \equiv \frac{V_e}{\overline{V}}$$

V_e local velocity in sheet at deflector exit, ft/sec

$\overline{V}$ average velocity at orifice exit, ft/sec

$\mathcal{W}$ mass distribution parameter, dimensionless;
$$\mathcal{M} \equiv \frac{d\dot{w}}{dx} \cdot \frac{144}{\rho \overline{V} d_0}$$

We Weber number, dimensionless; $We \equiv \dfrac{\overline{V}}{12} \sqrt{\dfrac{\rho d_0}{\sigma g_0}}$

$\dot{w}$ mass flow rate, lbm/sec

w overall sheet width as it leaves deflector, in. (Fig. 1)

x distance across sheet at any point, measured outward from centerline, in.

Greek

β sheet spreading angle, deg. (Fig. 1)

δ sheet deflection angle, deg. (Fig. 1)

ρ liquid density, lbm/ft^3

σ liquid surface tension, lbf/in.

θ deflector angle, deg. (Fig. 1)

μ liquid viscosity, $\dfrac{\text{lbm}}{\text{in.-sec}}$

References

1. Ingebo, R. D., "Drop-Size Distributions for Impinging-Jet Breakup in Airstreams Simulating the Velocity Conditions in Rocket Combustors," NACA TN 4222, 1958.

2. Johnson, B. H., "An Experimental Investigation of the Effects of Combustion on the Mixing of Highly Reactive Liquid Propellants," Technical Report 32-689, Jet Propulsion Laboratory, Pasadena, Calif., July 15, 1965.

3. Stanford, H. B., "Injector Development," Space Programs Summary 37-36, Vol. IV, pp. 174–176, Jet Propulsion Laboratory, Pasadena, Calif., December 31, 1965.

4. Evans, D. D., "Injector Development," Space Programs Summary 37-35, Vol. IV, pp. 152–155, Jet Propulsion Laboratory, Pasadena, Calif., October 31, 1965.

5. Powell, W. B., "Cup-and-Plug Injector Investigations," Space Programs Summary 37-31, Vol. IV, p. 203, Jet Propulsion Laboratory, Pasadena, Calif., January 31, 1965.

6. Rupe, J. H., "On the Dynamic Characteristics of Free-Liquid Jets and a Partial Correlation With Orifice Geometry," Technical Report 32-207, Jet Propulsion Laboratory, Pasadena, Calif., January 15, 1962.

7. LeClerc, A., "Deflection of a Liquid Jet By a Perpendicular Boundary," M.S. Thesis, University of Iowa, 1948.

8. Prandtl, L. and Tietjens, O. G., "Applied Hydro and Aero-Mechanics," McGraw-Hill Book Company, Inc., New York, 1934.

References (contd)

9. Riebling, R. W., "Controlling the Dimensions and Orientation of Impinging Propellant Sheets in Liquid Rocket Engine Injectors," Journal of Spacecraft and Rockets, Vol. 3, No. 11, pp. 1692–1694, November, 1966.

10. Riebling, R. W., "Injector Development," Space Programs Summary 37-41, Vol. V, Jet Propulsion Laboratory, Pasadena, Calif., October 31, 1966.

11. Riebling, R. W., "Injector Development," Space Programs Summary 37-44, Vol. V, Jet Propulsion Laboratory, Pasadena, Calif., May 31, 1967.